DISCRETE AND CONTINUOUS
DYNAMICAL SYSTEMS SERIES B
Volume **14**, Number **1**, July **2010**

doi:10.3934/dcdsb.2010.14.41

pp. **41–74**

A COLLOCATION METHOD FOR THE NUMERICAL FOURIER ANALYSIS OF QUASI–PERIODIC FUNCTIONS. I: NUMERICAL TESTS AND EXAMPLES

Gerard Gómez

Departament de Matemàtica Aplicada i Anàlisi
Universitat de Barcelona
Gran Via 585, 08007 Barcelona, Spain

Josep–Maria Mondelo

Departament de Matemátiques
Universitat Autónoma de Barcelona
Edifici C, 08193 Bellaterra (Barcelona), Spain

Carles Simó

Departament de Matemàtica Aplicada i Anàlisi
Universitat de Barcelona
Gran Via 585, 08007 Barcelona, Spain

(Communicated by Angel Jorba)

Abstract. The purpose of this paper is to develop a numerical procedure for the determination of frequencies and amplitudes of a quasi–periodic function, starting from equally–spaced samples of it on a finite time interval. It is based on a collocation method in frequency domain. Strategies for the choice of the collocation harmonics are discussed, in order to ensure good conditioning of the resulting system of equations. The accuracy and robustness of the procedure is checked with several examples. The paper is ended with two applications of its use as a dynamical indicator. The theoretical support for the method presented here is given in a companion paper [21].

1. **Introduction.** The goal of this paper is the development of a numerical method to solve the following frequency analysis problem: given N samples $\{f(jT/N)\}_{j=0}^{N-1}$ of a real-valued function $f(t)$, equally spaced on the interval $[0,T]$, determine a trigonometric polynomial,

$$Q_f(t) = A_0^c + \sum_{l=1}^{N_f} \big(A_l^c \cos(2\pi\nu_l t/T) + A_l^s \sin(2\pi\nu_l t/T) \big), \tag{1}$$

whose frequencies $\{\nu_l\}_{l=1}^{N_f}$, and amplitudes, $\{A_l^c\}_{l=0}^{N_f}$, $\{A_l^s\}_{l=1}^{N_f}$, are a good approximation of the ones of $f(t)$. The number of frequencies, N_f, has to be determined (in terms of some input parameters), and we want it to be as small as possible while keeping high accuracy in the frequencies and amplitudes computed.

2000 *Mathematics Subject Classification.* Primary: 58F15, 58F17; Secondary: 53C35.

Key words and phrases. Numerical Fourier analysis, Fast Fourier Transform, collocation method, quasi–periodic functions.

The procedure is based on some standard considerations on the discrete Fourier transform of a multi–frequency signal, in order to get a first approximation of frequencies and amplitudes, plus a collocation–like method in frequency domain, that improves this approximation.

Although the procedure does not explicitly assume real analyticity and quasi–periodicity of the input function, we will only consider this case. Our interest in this class of functions comes from its relevance in conservative dynamical systems. The KAM theorem [1, 2] shows that, for Hamiltonian dynamical systems that are sufficiently small perturbations of integrable ones, many trajectories can be parametrized by quasi–periodic functions. More recent work based on this type of techniques allows to show, for more general Hamiltonian systems (not necessarily small perturbation of integrable ones), the existence of families of quasi–periodic trajectories emanating from a known one (see [23] for theoretical results, and [34, 35, 36, 40, 41] for numerical explorations). These base trajectories can be an invariant torus of any dimension, in particular a periodic orbit or a fixed point. The procedure presented here allows to obtain a Fourier expansion of any of these trajectories directly from numerical simulation, which can be either simple iteration (in the case of discrete dynamical systems) or numerical integration of ODE (for continuous ones). This has proved to be useful in dynamical models related to astrodynamics (see [18, 19, 16, 17], where early versions of the present method have been used), such as the Restricted Three–Body Problem [42] or the Bi–circular Problem [39].

In many applications, one is not interested in a complete Fourier expansion of a trajectory, but in the evolution of the fundamental frequencies along a family of trajectories, in order to globally describe the behavior of the system. In this way, frequency analysis can be used as a dynamical indicator. Some examples of this kind of application are given later in this paper.

A classical approach to the frequency analysis problem stated above is to look for peaks of the discrete Fourier spectrum of the input signal, that is, of the modulus of its discrete Fourier transform (DFT). Each peak is then taken as an approximation of a frequency of the signal, whose amplitude is also approximated by the amplitude of the corresponding peak. This is useful in order to get a first estimate of frequencies and amplitudes, which can be sufficient in some applications, but will give errors in frequencies and amplitudes of the order of $1/T$, where T is the length of the interval of the samples.

There is an algorithm due to J. Laskar that improves this approximation. It is based on the realization that, if the input signal consists of a single complex periodic term, $f(t) = e^{i2\pi\nu t}$, the function

$$|a_k| := \left| \int_0^T f(t) e^{-i2\pi k t} dt \right|, \tag{2}$$

has a maximum at $k = \nu$. Therefore, ν can be computed by maximizing Eq. (2) with respect to k, which must be considered a real (non–integer) quantity. The peaks of the DFT can be taken as initial approximations for this maximization. In the case that the analyzed function has several periodic terms, each frequency perturbs the remaining ones by displacing the corresponding peaks, but this perturbation is expected to be small if the frequencies are not too close. This perturbation is reduced and, therefore, the precision of the method increased, if f is multiplied by a suitable window function before taking the integral in Eq. (2). The resulting

numerical procedure is known as *frequency map analysis* [25, 27, 26]. It has been successfully used as a dynamical indicator in many applications, either by using the variation of frequencies with time as a measure of diffusion, or by the detection of resonances through the analysis of ratios between the computed frequencies.

In [43, 44], a time–frequency analysis based on wavelets is presented. It is able to give the instantaneous frequencies associated with time series representing numerical trajectories of dynamical systems, producing the frequency evolution of the time–dependent variables of the system. Its main drawback is that the instantaneous frequencies (which, for periodic signals, are the Fourier frequencies) are defined only for analytic signals (a concept introduced by Gabor [13] and based on the Hilbert transform), and to determine if a given function is an analytic signal is not easy.

There is still another way to solve the frequency analysis problem, based on the construction of sequences of orthogonal polynomials known as *Szëgo polynomials* [22]. There are asymptotic results on the convergence of the zeros of these polynomials to the frequencies of the signal, but there are no explicit error estimates. Moreover, most of the development is done under the assumption that the number of frequencies in the signal is finite, and its implementation is rather cumbersome, compared to Laskar's procedure or the one presented in this paper.

The method presented in this paper combines the classical approach of frequency detection (looking for peaks of the DFT) with a collocation strategy in frequency domain, that allows to simultaneously improve all the frequencies and amplitudes detected. A main difference with respect to the one of Laskar is that, through this collocation strategy our procedure accounts for the displacements of the peaks of the Fourier spectrum due to the frequencies being computed, so that it is exact (except for roundoff) for finite trigonometric polynomials (see Section 3.5 for an example on this). In the case of an infinite number of frequencies (linear combinations of a finite basic set), the procedure is able to provide high precision while determining a small number of frequencies. In Section 4, a simple example is given in which the error in frequencies and amplitudes is of the order of 10^{-12}, whereas the number of computed frequencies is small enough as to have $\|f - Q_f\|_\infty \approx 10^{-2}$.

In a separate paper [21], we develop a complete error analysis for the procedure presented here, that produces computable bounds of the error in frequencies and amplitudes.

The paper is structured as follows. In Section 2 we introduce some notation and recall basic facts about Fourier analysis of discrete signals that are relevant in our development. The Fourier analysis procedure is presented in Section 3. It consists of three phases, that are first discussed separately in Subsections 3.1, 3.2, 3.3, and then combined in an iterative, general–purpose algorithm in Subsection 3.4. Section 3 ends with a very elementary example of application of the general–purpose algorithm of Subsection 3.4, introduced for a didactic purpose.

Section 4 is devoted to test the accuracy of the procedure using a family of analytic, quasi–periodic functions with known Fourier expansion. These functions depend on a parameter μ which allows to control the width of their band of analyticity around the real line and, hence, the (exponential) decreasing speed of their Fourier coefficients. Frequencies and amplitudes are computed for several values of T, N, and compared with the exact ones. The qualitative evolution of the error in terms of the T, N parameters is discussed, and related to the quantitative error

estimates given in [21]. We also test in this section the robustness of the procedure by introducing Gaussian noise in the input samples.

The paper is completed with two applications. The first one, in Section 5, is devoted to the detection of regular and chaotic motion in a family of symplectic 2D maps depending on a parameter. Both the initial actions and a large range of the parameter (where the main bifurcations occur) are scanned. The results are compared with those obtained with other dynamical indicators. The second application, in Section 6, studies the region of effective stability around the triangular points of the planar, circular Restricted Three–Body Problem for the Sun–Jupiter case. The Fourier method is used to reveal the resonant structure or this region, and to relate it to the frontier of the stability domain.

2. **Fourier analysis of discrete signals.** In this section we will introduce some notation and recall some standard considerations about Fourier analysis of discrete signals. For more details, see e.g. [3, 33, 14, 29].

Given a continuous signal $f(t)$, we will denote its normalized, windowed Fourier transform (NWFT) as

$$\phi_{f,T}(\omega) := \frac{1}{T}\int_0^T f(t)e^{-i2\pi\omega t}dt.$$

Here, the window function considered is the characteristic function of the interval $[0,T]$,

$$\chi_{[0,T]}(t) = \begin{cases} 1 & \text{if } t \in [0,T], \\ 0 & \text{otherwise.} \end{cases}$$

In this way $\phi_{f,T}(\omega) = \frac{1}{T}\widehat{\chi_{[0,T]}f}(\omega)$, where the hat symbol denotes the usual Fourier Transform (FT),

$$\hat{f}(\omega) = \int_{-\infty}^{\infty} f(t)e^{-i2\pi\omega t}dt. \tag{3}$$

Note that ω is not an angular frequency, due to the 2π factor in the exponent of the Fourier Transform in Eq. (3). Our frequency units will mostly be cycles per time unit.

A short calculation shows that the NWFT of a complex exponential term, $e^{i2\pi\nu t}$, is

$$\phi_{e^{i2\pi\nu t},T}(\omega) = \frac{e^{i2\pi(\nu-\omega)T}-1}{i2\pi(\nu-\omega)T}.$$

Since, for $x \in \mathbb{R}$

$$\left|\frac{e^{i2\pi x}-1}{i2\pi x}\right| = \left|\frac{\sin \pi x}{\pi x}\right| = |\operatorname{sinc} x|,$$

$|\phi_{e^{i2\pi\nu t},T}(\omega)|$ equals the modulus of a sinc function centered at the frequency ν (see Fig. 1 right). Comparing to the Fourier Transform of the same complex exponential term, which is a Dirac impulse based at ν (see Fig. 1 left), the frequencies with non–zero amplitudes in its NWFT can be considered a result of time truncation. This phenomenon is known as *leakage* in the literature.

If a signal consists of a sum of several complex exponential terms, leakage from each frequency perturbs the remaining ones, so that maxima at the highest peaks of $|\phi_{f,T}|$ are not exactly at the frequencies of the signal but slightly away (see Fig. 2). More concretely, if Ω is the set of frequencies of the signal, for every $\nu \in \Omega$ we have

$$f(t) = a_\nu e^{i2\pi\nu t} + \sum_{\xi\in\Omega\setminus\{\nu\}} a_\xi e^{i2\pi\xi t},$$

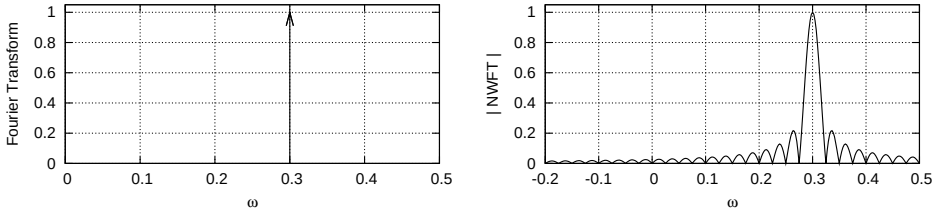

FIGURE 1. Left: FT of a complex exponential term $e^{i2\pi\nu t}$, for $\nu = 0.3$. Right: modulus of the NWFT of the same complex exponential term, for $T = 40$.

so that

$$|\phi_{f,T}(\omega)| = |a_\nu|\,|\operatorname{sinc}\big(T(\nu-\omega)\big)| + \sum_{\xi\in\Omega\setminus\{\nu\}} O\Big(\frac{1}{T(\xi-\omega)}\Big), \tag{4}$$

and the second term in the last equation is responsible for the peaks of $|\phi_{f,T}(\omega)|$ near $\omega = \nu$ not being exactly at ν. This term corresponds to leakage from the frequencies different from ν.

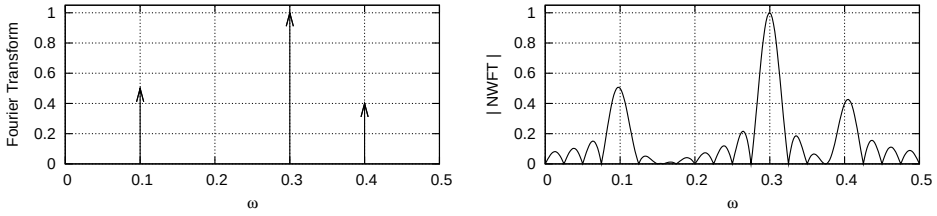

FIGURE 2. Left: modulus of the Fourier Transform of $0.5e^{i2\pi\nu_1 t} + e^{i2\pi\nu_2 t} + 0.4e^{i2\pi\nu_3 t}$, for $\nu_1 = 0.1$, $\nu_2 = 0.3$, $\nu_3 = 0.4$. It consists of three impulses, supported at ν_1, ν_2, ν_3. Right: modulus of the NWFT of the same function, for $T = 40$. Here, the leakage from each frequency prevents the higher peaks from being exactly at ν_1, ν_2, ν_3.

A usual strategy to reduce leakage is to replace $\chi_{[0,T]}(t)$ in the NWFT by a smoother window function (also called *filter* function). Among the window functions considered in the literature [3, 33, 14], Hanning's one is particularly useful for our purposes. We will denote the normalized (Hanning–)filtered, windowed Fourier transform with order n_h as

$$\phi^{n_h}_{f,T}(\omega) := \frac{1}{T}\int_0^T H^{n_h}_T(t) f(t) e^{-i2\pi\omega t} dt.$$

Here the Hanning filter function of order n_h is denoted as

$$H^{n_h}_T(t) = \begin{cases} q_{n_h}\Big(1 - \cos\dfrac{2\pi t}{T}\Big)^{n_h} & \text{if } t \in [0,T], \\ 0 & \text{otherwise,} \end{cases}$$

with

$$q_{n_h} = \frac{n_h!}{(2n_h-1)!!}. \tag{5}$$

A computation shows that

$$\phi^{n_h}_{e^{i2\pi\nu t},T}(\omega) = \frac{(-1)^{n_h}(n_h!)^2\big(e^{i2\pi(\nu-\omega)T}-1\big)}{i2\pi\prod_{j=-n_h}^{n_h}\big((\nu-\omega)T+j\big)} = O\Big(\frac{1}{\big((\nu-\omega)T\big)^{1+2n_h}}\Big), \qquad (6)$$

which is a significant reduction with respect to the error term in Eq. (4). This effect can also be understood qualitatively in terms of the regularity of the window function. The NWFT, which is the Fourier transform of the filtered input function $H^{n_h}(t)f(t)$, when sampled at the frequencies k/T, $k\in\mathbb{Z}$, gives the Fourier coefficients of the extension of $H^{n_h}(t)f(t)|_{[0,T]}$ to $\mathbb{R}$ by periodicity (see [3]). As n_h increases, the regularity of this periodic extension also increases (it is of class C^{2n_h+1} with a Lipschitz $(2n_h+1)$–th derivative), which implies a faster decreasing with $|k|$ of its Fourier coefficients and, therefore, of the NWFT.

Since our starting point is a finite number of samples, our procedure will not be based on the NWFT of the input signal but on its Discrete Fourier Transform (DFT), which will be denoted as

$$F_{f,T,N}(k) := \frac{1}{N}\sum_{j=0}^{N-1} f(jT/N)e^{-i2\pi kj/N}, \qquad (7)$$

for $k=0,1,\ldots,N-1$. We will also consider the Hanning–filtered DFT of order n_h,

$$F^{n_h}_{f,T,N}(k) := \frac{1}{N}\sum_{j=0}^{N-1} H^{n_h}_N(j)f(jT/N)e^{-i2\pi kj/N}. \qquad (8)$$

Note that the DFT is considered to be defined on harmonics $k\in\mathbb{Z}$, whereas the NWFT is defined on frequencies $\omega\in\mathbb{R}$.

The DFT and NWFT are related by

$$F^{n_h}_{f,T,N}(k) = \phi^{n_h}_{f,T}\Big(\frac{k}{T}\Big) + \sum_{l=1}^{\infty}\Big(\phi^{n_h}_{f,T}\Big(\frac{k+lN}{T}\Big) + \phi^{n_h}_{f,T}\Big(\frac{k-lN}{T}\Big)\Big), \qquad (9)$$

which, as it is stated, is true for $n_h\geq 1$ (see Lemma 2.2 in [21] for a comment on this). This formula states that the DFT at harmonics $k\in\mathbb{Z}$ is obtained by performing the N/T–periodification of the NWFT and sampling it at the frequencies k/T, $k\in\mathbb{Z}$ (see [3] for a graphical deduction). A consequence of this formula is that each term $e^{i2\pi\nu t}$ produces an infinite number of peaks in the DFT, at the harmonics $\lfloor T\nu+0.5\rfloor+jN$, $j\in\mathbb{Z}$ (note that $\lfloor -7.4\rfloor=-8$). One of the peaks will always be in the interval $[-N/2,N/2]$. Moreover, if the signal is real (which will always be our case), the Hermitian symmetry property of the DFT ($F^{n_h}_{f,T,N}(k)=\overline{F^{n_h}_{f,T,N}(-k)}$, where the overline symbol denotes complex conjugate) further restricts the fundamental frequency domain of the DFT to $[0,N/(2T)]$. Any frequency component of the signal will always produce a peak of the DFT in this interval.

Note in the previous argument the distinction between *harmonics* $k\in\mathbb{Z}$ and *frequencies* k/T, $k\in\mathbb{Z}$. We will maintain this convention from now on.

Eq. (9) ensures that the DFT is close to the NWFT for suitable harmonics (precise estimates are given in [21]). Consequently, given a frequency ν of the signal, if it satisfies $0<\nu<N/(2T)$, and if leakage from the rest of frequencies is not severe, there will be a peak of the modulus of the DFT close to $T\nu$, as it has been seen for the NWFT. When the signal has a frequency outside $[0,N/(2T)]$, and a peak of the DFT inside $[0,N/(2T)]$ is mistakenly considered an approximation of

this frequency, it is usual to speak about *aliasing*. In the literature, the error term of the DFT as approximation of the NWFT in Eq. (9) is also known as aliasing.

Since our procedure is based on the DFT, it can be affected by aliasing. A general strategy to deal with this fact is either to:

- be sure that we are not detecting frequencies greater than $N/(2T)$ cycles per time unit, or,
- if the signal has frequencies greater than $N/(2T)$ with relevant amplitudes, be aware of the fact that we will be detecting aliased frequencies. Actually, the true value of a frequency can be deduced from two aliases of it, corresponding to two samplings with different values of T.

Note that $N/(2T)$ is Nyquist's critical frequency in Shannon's sampling theorem.

3. **The Fourier analysis procedure.** In this section, our Fourier analysis procedure is developed. It consists of three phases:

- First approximation of frequencies, which is described in Subsection 3.1.
- Computation of (approximate) amplitudes from known frequencies, described in Subsection 3.2.
- Simultaneous improvement of frequencies and amplitudes, in Subsection 3.3.

Frequencies and amplitudes are not computed once, but iteratively detected and improved in blocks, starting from the largest–amplitude ones. In Subsection 3.4, an algorithm that describes this iterative process is given. This algorithm is illustrated through an example in Subsection 3.5.

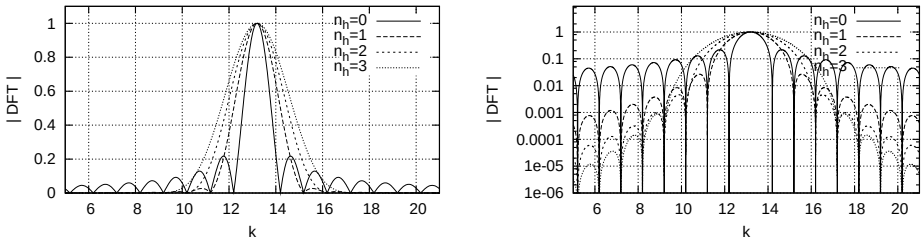

FIGURE 3. Modulus of the DFT of a complex exponential term, $|F^{n_h}_{e^{i2\pi\nu t},T,N}(k)|$, for $\nu = 0.33$, $T = N = 40$ and several values of n_h. It is seen how the width of the central peak broadens as n_h increases. In the right plot, logarithmic scale has been taken for the vertical axis.

3.1. **First approximation of frequencies.** In order to get a first approximation of the frequencies, we will follow the usual approach of looking for peaks of the DFT of the signal. From the samples of the input signal, $\{f(jT/N)\}_{j=0}^{N-1}$, its DFT coefficients, $\{F^{n_h}_{f,T,N}(k)\}_{k=0}^{N-1}$, can be computed by any standard FFT algorithm (see, e.g., [33, 10]). Then, given a minimum–amplitude tolerance $\bar{\delta}$ (whose choice is discussed in Subsection 3.4), for every harmonic $k \in \{1, \ldots, N/2-1\}$ satisfying

$$|F^{n_h}_{f,T,N}(k)| > \bar{\delta}, \qquad |F^{n_h}_{f,T,N}(k-1)| < |F^{n_h}_{f,T,N}(k)| > |F^{n_h}_{f,T,N}(k+1)|,$$

the harmonic k is taken as an approximate frequency of the signal in cycles per T time units. This will provide some approximate frequencies $\{\nu_0, \ldots, \nu_{N_f}\}$. At this

stage, one needs to be aware that, if N is not big enough, some of these frequencies can be close to aliased frequencies instead of true ones (see Section 2).

It is advisable to use the filtered DFT (that is, $n_h \geq 1$) in order to reduce leakage. Nevertheless, it is not convenient to take n_h too large. The peak of $F^{n_h}_{e^{i2\pi\nu t/T},T}$ around ν has width $2(1+n_h)$. This width refers to the distance between the two zeros of $F^{n_h}_{e^{i2\pi\nu t/T},T}(k)$ closest to $k=\nu$, see Fig. 3. For large n_h, the peaks of the modulus of the DFT corresponding to close frequencies could be mixed. Without further information, $n_h = 2$ is a good value to start with (see Section 2).

3.2. **Computation of amplitudes from known frequencies.** Once we have approximated frequencies, approximated amplitudes are found by a a collocation method in frequency domain. Namely, after choosing some harmonics, a linear system of equations is laid out by asking the DFT of the input data to be equal to the DFT of the current quasi–periodic approximation at the chosen harmonics. This system is then solved for the amplitudes.

Up to now we have used the complex form of the DFT. Nevertheless, since we will always use real signals, the method has been implemented in terms of sine and cosine transforms. For notational simplicity, we will always assume N to be even.

The Hanning–filtered, discrete sine and cosine transforms of a real signal f will be denoted as

$$\begin{aligned} c^{n_h}_{f,T,N}(k) &= \frac{2}{N}\sum_{j=0}^{N-1} f(jT/N)H^{n_h}_N(j)\cos\Big(2\pi\frac{k}{N}j\Big), \quad k=0,...,N/2, \\ s^{n_h}_{f,T,N}(k) &= \frac{2}{N}\sum_{j=0}^{N-1} f(jT/N)H^{n_h}_N(j)\sin\Big(2\pi\frac{k}{N}j\Big), \quad k=1,...,N/2-1. \end{aligned} \tag{10}$$

They are related to the complex DFT by

$$F^{n_h}_{f,T,N}(k) = \frac{1}{2}\Big(c^{n_h}_{f,T,N}(k) - is^{n_h}_{f,T,N}(k)\Big), \qquad k=0,\ldots,N/2.$$

Note that $s^{n_h}_{f,T,N}(0) = s^{n_h}_{f,T,N}(N/2) = 0$. For the special cases $f(t)=\cos(2\pi\nu t/T)$ and $f(t)=\sin(2\pi\nu t/T)$ needed in this section, we further note:

$$\begin{aligned} c^{n_h}_{1,N}(k) &= c^{n_h}_{1,T,N}(k), \\ \overline{c}^{n_h}_{\nu,N}(k) &= c^{n_h}_{\cos(\frac{2\pi\nu t}{T}),T,N}(k), \qquad \overline{s}^{n_h}_{\nu,N}(k) = s^{n_h}_{\cos(\frac{2\pi\nu t}{T}),T,N}(k), \\ \widetilde{c}^{n_h}_{\nu,N}(k) &= c^{n_h}_{\sin(\frac{2\pi\nu t}{T}),T,N}(k), \qquad \widetilde{s}^{n_h}_{\nu,N}(k) = s^{n_h}_{\sin(\frac{2\pi\nu t}{T}),T,N}(k). \end{aligned} \tag{11}$$

They can be evaluated from explicit formulae:

$$\begin{aligned} \overline{c}^{n_h}_{\nu,N}(k) &= \Re F^{n_h}_{e^{i2\pi\nu t/T},T,N}(k) + \Re F^{n_h}_{e^{i2\pi(-\nu)t/T},T,N}(k), \\ \overline{s}^{n_h}_{\nu,N}(k) &= -\Im F^{n_h}_{e^{i2\pi\nu t/T},T,N}(k) - \Im F^{n_h}_{e^{i2\pi(-\nu)t/T},T,N}(k), \\ \widetilde{c}^{n_h}_{\nu,N}(k) &= \Im F^{n_h}_{e^{i2\pi\nu t/T},T,N}(k) - \Im F^{n_h}_{e^{i2\pi(-\nu)t/T},T,N}(k), \\ \widetilde{s}^{n_h}_{\nu,N}(k) &= \Re F^{n_h}_{e^{i2\pi\nu t/T},T,N}(k) - \Re F^{n_h}_{e^{i2\pi(-\nu)t/T},T,N}(k), \\ F^{n_h}_{f,T,N}(k) &= \frac{q_{n_h}}{2^{n_h}}\sum_{m=-n_h}^{n_h}(-1)^m\binom{2n_h}{n_h+m}F_{f,T,N}(k+m), \end{aligned} \tag{12}$$

$$F_{e^{i2\pi\nu t/T},T,N}(k) = \frac{1-e^{i2\pi(\nu-k)}}{N(1-e^{i2\pi(\nu-k)/N})}.$$

with q_{n_h} defined as in Eq. (5). Eq. (12) follows from an application of the convolution theorem for the DFT (see e.g. [3, 14]) using the fact that

$$H_T^{n_h}(t) = \frac{q_{n_h}}{2^{n_h}} \sum_{m=-n_h}^{n_h} (-1)^m \binom{2n_h}{n_h+m} e^{i2\pi \frac{m}{T} t}.$$

A direct proof can be obtained by substitution of the previous expression in the definition of the DFT (Eq. (7)).

Now, if $\{\nu_1, \ldots, \nu_{N_f}\}$ are the approximated frequencies found in the previous section, and we denote by $\{k_1, \ldots, k_{N_f}\} \subset \{1, \ldots, N/2-1\}$ the harmonics chosen for collocation, a square linear system of equations for the amplitudes is obtained by imposing the condition

$$\left\{ \begin{array}{rcll} c^{n_h}_{Q_f,T,N}(0) & = & c^{n_h}_{f,T,N}(0), & \\ c^{n_h}_{Q_f,T,N}(k_j) & = & c^{n_h}_{f,T,N}(k_j), & j = 1, \ldots, N_f, \\ s^{n_h}_{Q_f,T,N}(k_j) & = & s^{n_h}_{f,T,N}(k_j), & j = 1, \ldots, N_f, \end{array} \right.$$

where Q_f is the current quasi–periodic approximation of the input signal, defined as in Eq. (1). Note that the units of ν_i correspond to Eq. (1), that is, they are in cycles per T time units (the reason for this is to have independence with respect to T in the sine and cosine transforms of sines and cosines of Eq. (11)). Using linearity of the DFT, we can expand the left–hand side of the previous system in order to obtain

$$\begin{aligned} A_0^c c^{n_h}_{1,N}(0) \; + \; \sum_{l=1}^{N_f} \big(\, A_l^c \overline{c}^{n_h}_{\nu_l,N}(0) \; + \; A_l^s \widetilde{c}^{n_h}_{\nu_l,N}(0) \, \big) \; &= \; c^{n_h}_{f,T,N}(0), \\ A_0^c c^{n_h}_{1,N}(k_j) \; + \; \sum_{l=1}^{N_f} \big(A_l^c \overline{c}^{n_h}_{\nu_l,N}(k_j) \; + \; A_l^s \widetilde{c}^{n_h}_{\nu_l,N}(k_j) \big) \; &= \; c^{n_h}_{f,T,N}(k_j), \\ \sum_{l=1}^{N_f} \big(A_l^c \overline{s}^{n_h}_{\nu_l,N}(k_j) \; + \; A_l^s \widetilde{s}^{n_h}_{\nu_l,N}(k_j) \big) \; &= \; s^{n_h}_{f,T,N}(k_j), \end{aligned} \tag{13}$$

with $j = 1, \ldots, N_f$. In this way we get a $(1+2N_f) \times (1+2N_f)$ linear system. Its coefficient matrix is computed from the explicit formulae of Eq. (11). Its right–hand side is evaluated from the DFT of the input data $\{f(jT/N)\}_{j=1}^{N-1}$.

The collocation harmonics k_j still have not been specified. A natural choice is

$$k_i = \lfloor \nu_i + 0.5 \rfloor,$$

in order to have $|k_i - \nu_i| \leq 1/2$ for $i = 1, \ldots, N_f$. Since the DFT of a sine or a cosine with frequency ν (in cycles per T time units) evaluated at an harmonic k decreases as $|\nu - k|$ goes away from zero (except for aliasing), this system is not only invertible but close to block–diagonal (if N is large enough in order to avoid aliasing). Therefore, it is well conditioned. In [21], a bound is provided for the norm of the inverse of its coefficient matrix. If computational speed is an issue, the structure of this system is very well suited for a 2×2 block Jacobi method, for which very fast convergence can be deduced from the bounds given in [21]. See also [19] for more details.

3.3. **Improvement of frequencies and amplitudes.** The same collocation idea of the previous section allows to improve the approximations of frequencies and amplitudes. Since now we will also solve for the frequencies, an additional equation is needed for each frequency, in order to get a square system. The resulting system of equations is no longer linear, and can be solved by Newton's method.

Concretely, we solve for $\{\nu_l\}_{l=1}^{N_f}$, $\{A_l^c\}_{l=0}^{N_f}$, $\{A_l^s\}_{l=1}^{N_f}$ the following non–linear system of equations:

$$\begin{aligned}
A_0^c c_{1,N}^{n_h}(0) \;+\; \sum_{l=1}^{N_f}\Big(\quad A_l^c \overline{c}_{\nu_l,N}^{n_h}(0) \;+\; A_l^s \widetilde{c}_{\nu_l,N}^{n_h}(0) \quad\Big) &= c_{f,T,N}^{n_h}(0),\\
A_0^c c_{1,N}^{n_h}(k_j) \;+\; \sum_{l=1}^{N_f}\Big(\quad A_l^c \overline{c}_{\nu_l,N}^{n_h}(k_j) \;+\; A_l^s \widetilde{c}_{\nu_l,N}^{n_h}(k_j) \quad\Big) &= c_{f,T,N}^{n_h}(k_j),\\
\sum_{l=1}^{N_f}\Big(\quad A_l^c \overline{s}_{\nu_l,N}^{n_h}(k_j) \;+\; A_l^s \widetilde{s}_{\nu_l,N}^{n_h}(k_j) \quad\Big) &= s_{f,T,N}^{n_h}(k_j),\\
A_0^c cs_{1,N}^{n_h}(k_j^+) \;+\; \sum_{l=1}^{N_f}\Big(A_l^c \overline{cs}_{\nu_l,N}^{n_h}(k_j^+) \;+\; A_l^s \widetilde{cs}_{\nu_l,N}^{n_h}(k_j^+)\Big) &= cs_{f,T,N}^{n_h}(k_j^+),
\end{aligned} \tag{14}$$

with $j = 1, \ldots, N_f$. In the above system of equations, cs denotes either c or s. A simple criterion to choose one or the other is to minimize a norm of the inverse of the 3×3 block $B_{j,j}$ defined in Eq. (15) (see [21] for the theoretical justification of this choice). The collocation harmonics, k_j and k_j^+, are chosen as the closest integers to the frequency ν_j. Namely,

$$\begin{aligned}
&k_j = \lfloor \nu_j \rfloor,\ k_j^+ = \lfloor \nu_j \rfloor + 1, && \text{if } \nu_j - \lfloor \nu_j \rfloor \le 1/2,\\
&k_j = \lfloor \nu_j \rfloor + 1,\ k_j^+ = \lfloor \nu_j \rfloor, && \text{otherwise.}
\end{aligned}$$

Assume $k_j \ge 1 + n_h$ for $j = 1 \div N_f$, so that, from Eq. (12), we have $c_{1,N}^{n_h}(k_j) = 0$. With the unknowns ordered as

$$A_0^c,\ \nu_1,\ A_1^c,\ A_1^s,\ \ldots,\ \nu_{N_f},\ A_{N_f}^c,\ A_{N_f}^s,$$

the differential of Eq. (14), which is needed to apply Newton's method, can be written as

$$M = \begin{pmatrix} 2 & v_1 & \cdots & v_{N_f} \\ 0 & B_{1,1} & \cdots & B_{1,N_f} \\ \vdots & \vdots & \ddots & \vdots \\ 0 & B_{N_f,1} & \cdots & B_{N_f,N_f} \end{pmatrix},$$

being

$$\begin{aligned}
v_l &= \begin{pmatrix} A_l^c \partial \overline{c}_{\nu_l,N}^{n_h}(0) + A_l^s \partial \widetilde{c}_{\nu_l,N}^{n_h}(0) & \overline{c}_{\nu_l,N}^{n_h}(0) & \widetilde{c}_{\nu_l,N}^{n_h}(0) \end{pmatrix},\\
B_{j,l} &= \begin{pmatrix} A_l^c \partial \overline{c}_{\nu_l,N}^{n_h}(k_j) + A_l^s \partial \widetilde{c}_{\nu_l,N}^{n_h}(k_j) & \overline{c}_{\nu_l,N}^{n_h}(k_j) & \widetilde{c}_{\nu_l,N}^{n_h}(k_j) \\ A_l^c \partial \overline{s}_{\nu_l,N}^{n_h}(k_j) + A_l^c \partial \overline{s}_{\nu_l,N}^{n_h}(k_j) + A_l^s \partial \widetilde{s}_{\nu_l,N}^{n_h}(k_j) & \overline{s}_{\nu_l,N}^{n_h}(k_j) & \widetilde{s}_{\nu_l,N}^{n_h}(k_j) \\ A_l^c \partial \overline{cs}_{\nu_l,N}^{n_h}(k_j^+) + A_l^s \partial \widetilde{cs}_{\nu_l,N}^{n_h}(k_j^+) & \overline{cs}_{\nu_l,N}^{n_h}(k_j^+) & \widetilde{cs}_{\nu_l,N}^{n_h}(k_j^+) \end{pmatrix}
\end{aligned} \tag{15}$$

where ∂ denotes derivative with respect to ν. As in the preceding section, due to the choice of the collocation harmonics, this matrix is close to block–diagonal and, therefore, the system to be solved at each Newton iteration is well conditioned.

Since the phases of the procedure described in the previous subsections are used only in order to get first approximations, the error of the whole procedure is the difference between the true frequencies and amplitudes of the input function and the ones obtained solving the system of Eq. (14). The only source of error (apart from roundoff) is leakage from the frequencies that we are not approximating. More concretely: if in the system of Eq. (14), the right–hand side is the DFT of the trigonometric polynomial formed by the exact frequencies and amplitudes we want to determine (evaluated at the collocation harmonics), we will obtain the exact frequencies and amplitudes as a solution. The system of Eq. (14) is obtained from this "exact" system by perturbing its right–hand side by the DFT of the remaining frequencies of the signal, evaluated at the collocation harmonics.

Note that the combination of the procedures of Subsections 3.1 and 3.2 is not satisfying this "exactness" property, and neither are other methods for frequency analysis mentioned at the Introduction.

3.4. **A general purpose algorithm.** In order to prevent some frequencies to hide nearby frequencies of lower amplitude, the three phases described above are not applied just once in order to find a prescribed number of frequencies and amplitudes. Instead of that, the analysis is carried out as an iterative process, so that at each iteration we apply the three phases previously described to frequencies whose amplitude is greater than a given tolerance $\bar{\delta}$. This tolerance is decreased in each iteration, up to a prescribed minimum. More concretely, if we want to capture frequencies up to an amplitude b_{min} and p_{max} is the largest peak in the DFT, one can define $\delta = (b_{min}/p_{max})^{1/n}$, where n is the number of iterations of the procedure, and then at the i-th step we take $\bar{\delta} = p_{max} \times \delta^i$.

Algorithm 3.1 is a general–purpose algorithm that implements this iterative process[1]. For brevity, in this algorithm we use the *power spectral density* (PSD),

$$p^{n_h}_{f,T,N}(k) \;=\; \left((c^{n_h}_{f,T,N}(k))^2 + (s^{n_h}_{f,T,N}(k))^2\right)^{1/2}, \qquad k = 0, \ldots, N/2.$$

Note that, at each iteration, steps 2 and 3 of the procedure are applied to *all* the frequencies and amplitudes, instead of just to the new ones.

Algorithm 3.1. *Given*

T	*(length of the time interval of the samples),*
N	*(number of samples),*
$\{f(j\frac{T}{N})\}_{j=0}^{N-1}$	*(samples of the function to be analyzed),*
n_h	*(Hanning order for filtering),*
$N_{f\,max}$	*(maximum number of frequencies to be determined),*
b_{min}	*(minimum amplitude for the frequencies to be computed),*
n	*(number of iterations for the procedure),*
tol_t	*(signal domain stopping tolerance),*
tol_f	*(power spectral domain stopping tolerance),*

compute the frequencies and amplitudes $\{\nu_j\}_{j=1}^{N_f}$, $\{A^c_j\}_{j=0}^{N_f}$, $\{A^s_j\}_{j=1}^{N_f}$ *of a quasi–periodic approximation of* f*,*

$$Q_f(t) := A^c_0 + \sum_{l=1}^{N_f}\Big(A^c_l \cos(2\pi\frac{\nu_l}{T}t) + A^s_l \sin(2\pi\frac{\nu_l}{T}t)\Big),$$

as follows:

[1] A C routine implementing this algorithm is available upon request to `jmm@mat.uab.cat`

$p_{max} :=\max_{j=1\div N/2} p^{n_h}_{f,T,N}(j)$
$\delta := (b_{min}/p_{max})^{1/n}$
$Q_f(t) := 0$
$N_f := 0$
for i **from** 1 **to** n **do**
  if $N_f \geq N_{f\,max}$ **then**
    STOP (maximum number of frequencies reached)
  end if
  Compute the peaks of the PSD of $f - Q_f$ *with amplitude* $\geq p_{max}\delta^i$,
    but without exceeding a total maximum of $N_{f\,max}$ *frequencies.*
    Let them be $\{k_{N_f+1}, \ldots, k_{N_f+m}\}$.
  if *there exist* $0 \leq l_1, l_2 \leq N_f + m$ *such that* $|k_{l_1} - k_{l_2}| < 2 + n_h$ **then**
    STOP (frequencies too close)
  end if
  Apply Section 3.1: take $\{\nu_{N_f+1}, \ldots, \nu_{N_f+m}\} = \{k_{N_f+1}, \ldots k_{N_f+m}\}$.
  Apply Section 3.2 to compute $\{A^c_l\}_{l=0}^{N_f+m}$, $\{A^s_l\}_{l=1}^{N_f+m}$ *from* $\{\nu_l\}_{l=1}^{N_f+m}$
  Apply Section 3.3 to improve $\{\nu_l\}_{l=1}^{N_f+m}$, $\{A^c_l\}_{l=0}^{N_f+m}$, $\{A^s_l\}_{l=1}^{N_f+m}$
  $N_f := N_f + m$
  $Q_f(t) := A^c_0 + \sum_{l=1}^{N_f} \big(A^c_l \cos(2\pi\nu_l t/T) + A^s_l \sin(2\pi\nu_l t/T)\big)$
  if $\max_{j=1,\ldots,N/2-1} \big(p^{n_h}_{f-Q_f,T,N}(j)\big) < \mathrm{tol}_f$ **then**
    STOP
  end if
  if $\max_{j=0,\ldots,N-1} |f(t_j) - Q_f(t_j)| < \mathrm{tol}_t$ **then**
    STOP
  end if
end for

In an actual implementation of the procedure, some technical details have to be taken into account, concerning:

- The use of stable trigonometric recurrences for the computation of $\{\cos mx, \sin mx\}_{m=0}^{N/2}$, in order to avoid unnecessary calls to the sin and cos functions of the math library.
- The avoidance of cancellations in the evaluation of the discrete sine and cosine transforms of sines and cosines defined in Eq. (11).

For these technical details, see [31].

As it has been mentioned in the introduction, the numerical Fourier analysis procedure does not assume that f is quasi–periodic, but in applications we will always assume that this is the case. A quasi–periodic function f has a Fourier expansion of the form

$$f(t) = \sum_{k\in\mathbb{Z}^m} a_k e^{i2\pi\langle k,\omega\rangle t},$$

with $\omega = (\omega_1, \ldots, \omega_m)$ a vector of rationally independent basic frequencies. A set of basic frequencies satisfies that all the frequencies detected in the signal are integer linear combinations of the basic frequencies and it is minimal with this property. It is not unique: given a set of basic frequencies, any other set obtained from it by applying a unimodular matrix is also basic.

Algorithm 3.1 gives individual frequencies, but does not distinguish between basic and non–basic ones. If a basic frequency set is required, it must be determined

a posteriori. Simple strategies, like the one depicted in Algorithm 3.2 are often satisfactory. This algorithm has been used for the determination of basic frequencies in Section 6.

Algorithm 3.2. *Given*

$\{\omega_1, \ldots, \omega_{N_f}\}$	*(frequencies),*
$\mathrm{tol} < \mathrm{tol}_2$	*(tolerances),*
$\mathrm{or}_{\max}$	*(maximum order for linear combinations)*
$m_{\max}$	*(maximum number of basic frequencies allowed),*

compute

m	*(number of (needed) basic frequencies),*
$\{b_1, \ldots, b_m\} \subset \{1, \ldots, N_f\}$	*(indexes of the basic frequencies, so that the basic frequencies will be* $\{\omega_{b_1}, \ldots, \omega_{b_m}\}$*),*
$\{(k_0^j, k_1^j, \ldots, k_m^j)\}_{j=1}^{N_f}$	*(coefficients for linear combinations),*

with the coefficients $\{(k_0^j, k_1^j, \ldots, k_m^j)\}_{j=1}^{N_f}$ *satisfying*

$$|k_0^i\omega_i + k_1^i\omega_{b_1} + k_2^i\omega_{b_2} + \cdots + k_m^i\omega_{b_m}| < \mathrm{tol}_2,$$

as follows:

$b_1 := \omega_1, \quad (k_0^1, k_1^1) := (-1, 1), \quad \mathrm{err}_1 := 0, \quad \mathrm{or}_1 := 1$
for $i = 2, \ldots, N_f$ do
  $\big(\mathrm{err}_i, \mathrm{or}_i, \{k_1^i, \ldots, k_m^i\}\big) :=$ **adjust**$(\omega_i, \{\omega_{b_j}\}_{j=1}^m, \mathrm{or}_{\max}, \mathrm{tol})$
  if $|\mathrm{err}_i| \geq \mathrm{tol}_2$ *and* $m < m_{\max}$ **then**
    $m := m + 1$, $b_m := i$
    for $j = 1, \ldots, i-1$ **do** $k_m^j := 0$ **endfor**
    $(k_0^i, k_1^i, \ldots, k_{m-1}^i, k_m^i) = (-1, 0, \ldots, 0, 1)$
    $\mathrm{err}_i := 0$, $\mathrm{or}_i := 1$
  endif
endfor

This algorithm assumes a function

$$(\mathrm{err}, \mathrm{or}, \{k_0, \ldots, k_m\}) = \textbf{adjust}(\omega, \{\omega_1, \ldots, \omega_m\}, \mathrm{or}_{\max}, \mathrm{tol})$$

whose objective is to find $\{k_0, \ldots, k_m\}$ with $|k_0| + |k_1| + \cdots + |k_m| \leq \mathrm{or}_{\max} + 1$ satisfying

$$|k_0\omega + k_1\omega_1 + \cdots + k_m\omega_m| < \mathrm{tol}. \tag{16}$$

For that, all the coefficients $k = (k_1, \ldots, k_m)$ with $|k_1| + \cdots + |k_m| \leq \mathrm{or}_{\max}$ need to be generated and tried. The k_0 coefficient can be computed from the m–tuple k as

$$k_0 = \lfloor(-k_1\omega_1 - \cdots - k_m\omega_m)/\omega + 0.5\rfloor$$

where $\lfloor\ \rfloor$ denotes integer part. A convenient ordering for the generation of k is by increasing order and lexicographically within each order. If coefficients are found satisfying Eq. (16), the **adjust** function must return immediately. Otherwise, it has to try all m–tuples k up to order $\mathrm{or}_{\max}$, and return the one with minimum error. This error has to be returned as err, and $|k_0| + |k_1| + \cdots + |k_m| - 1$ as or.

Two useful quantities to be returned by a routine implementing the previous algorithm are

$$\max_{i=1,\ldots,N_f} \mathrm{err}_i, \qquad \max_{i=1,\ldots,N_f} \mathrm{or}_i.$$

In principle the selection of basic frequencies is based on the ones which are independent (with the prescribed tolerance) and have the largest amplitude. But it can be also desirable to change the basic set in order to have a regular *continuation* of the basic frequencies with respect to parameters. On the other hand, it can happen that the number of *needed* basic frequencies is less than the *expected or maximal* number of basic frequencies. For instance, in an r-degrees of freedom Hamiltonian depending quasi–periodically on time with s external frequencies, one could expect to have quasi–periodical solutions having $r+s$ basic frequencies, but the real value can be smaller.

3.5. **An illustration of the procedure.** In this subsection, we display intermediate computations corresponding to the application of Algorithm 3.1 to the following signal:

$$f(t) = \cos(2\pi 0.13t) - \frac{1}{2}\sin(2\pi 0.27t) + \frac{3}{4}\sin(2\pi 0.41t),$$

with $T = N = 64$ and $n_h = 2$. These computations are shown just for illustrating purposes, and by no means are intended as a typical example of application of the procedure. Further applications can be found in the forthcoming sections.

For simplicity, frequencies will be given in cycles per time unit, instead of the units in which they are computed (cycles per T time units). The values of the rest of parameters of Algorithm 3.1 used for this example are:

$$\mathrm{tol}_f = 10^{-12}, \quad n = 2, \quad b_{min} = 0.45, \quad N_{f_{max}} = 10, \quad \mathrm{tol}_t = 10^{-12}.$$

1. Starting amplitude threshold: 0.657358
   Modulus of the DFT of the input data:

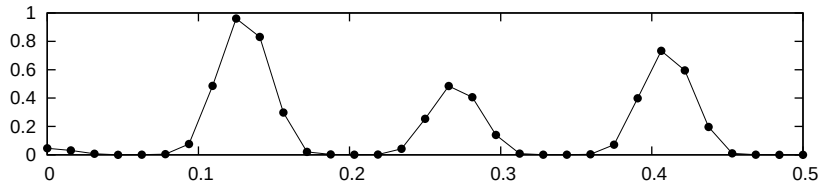

2. First approximation of frequencies (Section 3.1):

   peak 8 $\Rightarrow$ frequency 0.1250000000000000
   peak 26 $\Rightarrow$ frequency 0.4062500000000000

3. Computation of approximated amplitudes for the approximated frequencies (Section 3.2):

Frequency	Cosine amplitude	Sine amplitude
0.1250000000000000	0.5145306752835769	−0.8107824606608708
0.4062500000000000	0.5018521508131750	0.5344214448451747

   Modulus of the DFT of the residual (input function minus quasi–periodic approximation):

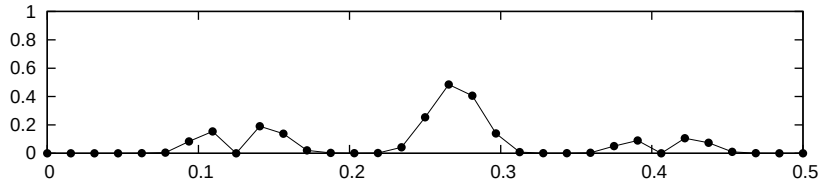

Note the central peak, corresponding to the frequency 0.27, still to be detected, and the two lateral "volcanoes", due to the poor approximation of the 0.13 and 0.41 frequencies.

4. Improvement of frequencies and amplitudes (Section 3.3):

Frequency	Cosine amplitude	Sine amplitude
0.1299996460498701	0.9999951867855691	−0.0000789912634604
0.4099995983712129	0.0000620281167449	0.7500069020136115

Note that, according to Eq. (4), the perturbation of the frequency 0.27 (still not detected) on the frequency 0.41 is $O\big(1/(0.1T)^5\big) = O\big(0.91 \times 10^{-4}\big)$. The observed error is approximately 66% of this quantity.

5. Modulus of the DFT of input signal minus the current quasi–periodic approximation:

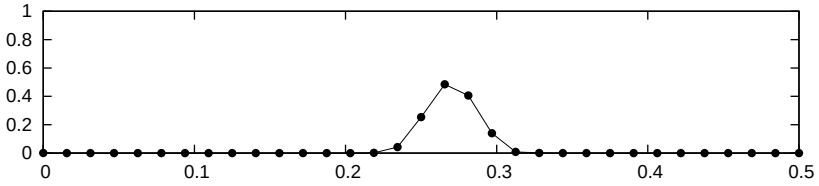

Note that the volcanoes are gone.

New amplitude threshold: 0.45

6. First approximation of frequencies (Section 3.1):

$$\text{peak } 17 \quad \Rightarrow \text{frequency } 0.2656250000000000$$

7. Approximated amplitudes from approximated frequencies (Section 3.2):

Frequency	Cosine amplitude	Sine amplitude
0.1299996460498701	0.9999951867855691	−0.0000789912634587
0.4099995983712129	0.0000620281167456	0.7500069020136115
0.2656250000000000	−0.3734879006102361	−0.3089760741255307

Modulus of the DFT of the residual

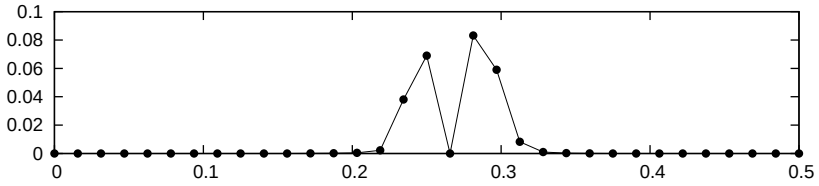

8. Iterative refinement of frequencies and amplitudes (Section 3.3):

Frequency	Cosine amplitude	Sine amplitude
0.1300000000000000	0.9999999999999994	0.0000000000000007
0.4099999999999999	0.0000000000000040	0.7499999999999996
0.2700000000000000	−0.0000000000000042	−0.4999999999999995

Note that now the only error is rounding.

Modulus of the DFT of the residual:

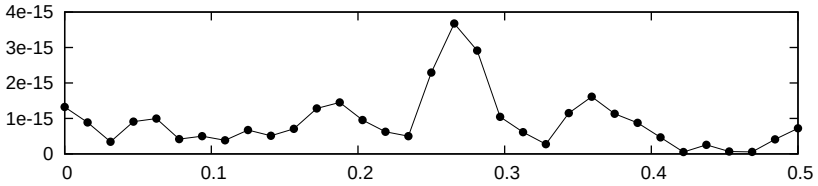

Note that it is of the order of (double–precision) roundoff error.

9. The algorithm stops because $\max_{j=1,\dots,N/2}\big(p^{n_h}_{f-Q_f,T,N}(j)\big) < \mathrm{tol}_f$.

4. **A test for the accuracy and robustness of the procedure.** This section is devoted to a second example that illustrates the accuracies that the procedure can reach. We perform an exploration, varying the T, N parameters, of a family of quasi–periodic functions with known Fourier expansions. This family of functions depends on a parameter μ that controls the width of the analyticity band of the functions in the family, and hence the decreasing speed of their Fourier coefficients. In order to test the robustness of the procedure, an additional exploration is performed adding Gaussian noise to the function samples.

The quasi–periodic functions considered depend on a parameter μ, a frequency vector $\omega = (\omega_1, \dots, \omega_m)$, and two phase vectors $\varphi = (\varphi_1, \dots, \varphi_m)$, $\widetilde{\varphi} = (\widetilde{\varphi}_1, \dots, \widetilde{\varphi}_m)$. They are defined as

$$f_\mu(t) = \prod_{j=1}^{m} \frac{\sin(2\pi\omega_j t + \varphi_j)}{1 - \mu\cos(2\pi\omega_j t + \widetilde{\varphi}_j)} = \sum_{k\in\mathbb{Z}^m} a_k^{\varphi,\widetilde{\varphi}} e^{i2\pi\langle k,\omega\rangle t}, \qquad \mu \in [0,1),$$

with $a_k^{\varphi,\widetilde{\varphi}} = a_{1,k_1}^{\varphi_1,\widetilde{\varphi}_1} a_{2,k_2}^{\varphi_2,\widetilde{\varphi}_2} \dots a_{m,k_m}^{\varphi_m,\widetilde{\varphi}_m}$, being

$$a_{j,k_j}^{\varphi_j,\widetilde{\varphi}_j} = \frac{e^{ik_j\widetilde{\varphi}_j}}{\mu}\left(\frac{1-\sqrt{1-\mu^2}}{\mu}\right)^{|k_j|}\left(\frac{\sin(\varphi_j - \widetilde{\varphi}_j)}{\sqrt{1-\mu^2}} - i\,\mathrm{sig}(k_j)\cos(\varphi_j - \widetilde{\varphi}_j)\right), \quad (17)$$

if $k_j \neq 0$, and

$$a_{j,k_j}^{\varphi_j,\widetilde{\varphi}_j} = \frac{\mu\sin(\varphi_j - \widetilde{\varphi}_j)}{1-\mu^2+\sqrt{1-\mu^2}}, \quad (18)$$

if $k_j = 0$. The phases φ and $\widetilde{\varphi}$ do not play any other role than to break symmetries in the Fourier expansions.

We have applied Algorithm 3.1 to the f_μ functions for $m = 2$, $\omega = (1, \sqrt{2})$, $\varphi = (\sqrt{0.2}, \sqrt{0.3})$, $\widetilde{\varphi} = (\sqrt{0.4}, \sqrt{0.5})$, $n_h = 2$ and several values of μ, T, N, with T, N ranging over powers of 2. We have stopped the procedure when all the frequencies of order $|k| \leq 5$ have been obtained.

In Fig. 4 we represent the maximum difference (in absolute value) between the true frequencies and amplitudes and the computed ones. In order to compare the error in frequencies corresponding to analysis with different values of T, we have used cycles per time unit (Hertz, if time is in seconds) as frequency units for this comparison, instead of the units in which frequencies are computed. In this way, for each analysis, if $\{\widetilde{\nu}_j\}_{j=1}^{N_f}$, $\{\widetilde{A}_j^c\}_{j=0}^{N_f}$, $\{\widetilde{A}_j^s\}_{j=1}^{N_f}$ are the frequencies and amplitudes given by Algorithm 3.1, and $\{\nu_j\}_{j=1}^{N_f}$, $\{A_j^c\}_{j=0}^{N_f}$, $\{A_j^s\}_{j=1}^{N_f}$ are the exact ones (given by Eqs. (17, 18)), in Fig. 4 we represent, for each analysis,

$$\max\Big(\max_{j=1,\dots,N_f}|(\widetilde{\nu}_j - \nu_j)/T|, \max_{j=0,\dots,N_f}|\widetilde{A}_j^c - A_j^c|, \max_{j=1,\dots,N_f}|\widetilde{A}_j^s - A_j^s|\Big).$$

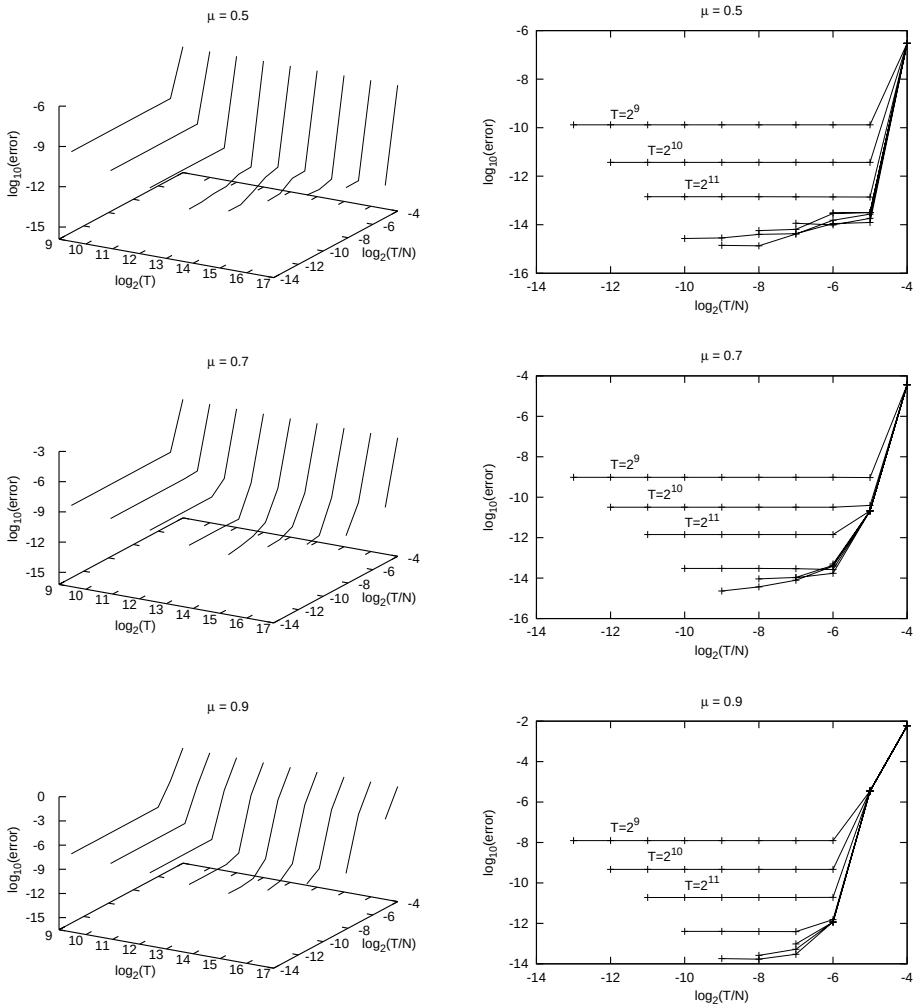

FIGURE 4. Error in the Fourier analysis of the f_μ functions for $\mu = 0.5, 0.7, 0.9$. The maximum error in frequencies and amplitudes is represented with respect to the parameters T, N. Points corresponding to analysis with the same value of T have been joined by lines. The right–hand figures are the (y, z) projection of the left–hand side ones.

A first observation is that the error in frequencies and amplitudes is much smaller than the difference between the analyzed function f and its computed quasi–periodic approximation Q_f. For instance, in the case of $\mu = 0.9$, from Eqs. (17, 18) the maximum amplitude of the non–computed frequencies is 0.0843, whereas we reach errors as small as nearly 10^{-14} for some values of T and N. This is due to the fact that the truncation error of our procedure is not introduced by the difference $f - Q_f$ but by its DFT.

We also observe that, for every value of T, as N increases the error decreases and becomes constant after a value of N. We also note that the minimum error for each

value of T decreases as we increase T. This behavior of the error in terms of the parameters T, N, can be qualitatively explained in terms of leakage and aliasing. Namely:

- For fixed T and increasing N, the error decreases and stabilizes after a value of N. The error for low values of N is due to aliasing of low–order (and therefore not necessary of small amplitude) frequencies not being determined, and the fact that the error in our method comes from leakage of these frequencies (see the end of Subsection 3.3). More concretely, for N not large enough, there are low–order frequencies not being computed which are outside $[0, N/(2T)]$. Therefore, they have aliases inside $[0, N/(2T)]$, and it may happen that one of the collocation harmonics is near one of this aliases. In this case, its DFT, evaluated at this harmonic, may not be small (in [21], this corresponds to the term of the bound of $\|\Delta b\|$ that contains D_a^* in the denominator). As N increases, the frequencies outside $[0, N/(2T)]$ are of high order, so they have small amplitudes and their aliases inside $[0, N/(2T)]$ are not harmful.
- The minimum error for each T decreases as T increases because the leakage from the frequencies not being computed does the same (see Eq. (6)).

4.1. **The effect of noise.** In order to test the robustness of the procedure, we have repeated a part of the previous Fourier exploration of the f_μ functions adding Gaussian noise to their samples, with zero mean and standard deviation $\Delta/2$. We have used the same values of $m, \omega, \varphi, \widetilde{\varphi}$ as before, $\mu = 0.7$, $T = 8192$, and several values of N and Δ. N has varied over powers of 2 from 2^{17} to 2^{22}, whereas Δ has varied from 10^{-2} to 10^{-10} over powers of 10^{-1}.

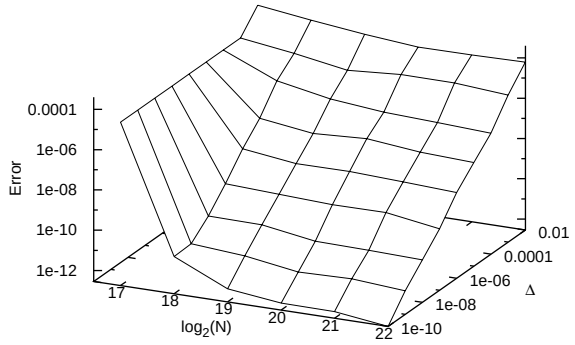

FIGURE 5. Fourier analysis of the f_μ functions, $\mu = 0.7$, $T = 8192$, with Gaussian noise. To each sample of f_μ, we have added a normal deviate with mean 0 and standard deviation $\Delta/2$.

The results can be seen in Fig. 5. For increasing N and fixed values of Δ, with exception of the largest ones, we can observe the same qualitative behaviour as in Fig. 5. The non–decreasing of the error with N for large Δ can be attributed to the effect of the noise being comparable to the effect of aliasing for low values of N. From $N = 2^{19}$ on and for fixed values of N, the error can be observed to approximately behave as $10^{-2}\Delta$.

5. **A dynamical application: detection of regular and chaotic motion.** This second example is related to the application of frequency analysis to distinguish between regular and chaotic motion in a dynamical system. This use of frequency analysis as an indicator of the dynamics is one of its most popular applications up to date (see, e.g., [25],[26]). The basic idea is to take two samples of an orbit on disjoint time intervals and perform frequency analysis. If we obtain the same frequencies in both intervals, the orbit is considered regular. Otherwise it is considered chaotic. This procedure is applied over a representative set of orbits of the dynamical system under study.

More concretely, consider a dynamical system in dimension d, either continuous ($x(t) = \varphi(t, x(0))$) or discrete ($x(n) = T^n(x(0))$). Take different initial conditions $x(0)$, for instance along some line or sub–manifold, and compute the corresponding orbits for some time interval or for some number of iterates. In the continuous case, we sample the orbits at times of the form $t_j = j\Delta t$, $j = 0, 1, 2, \ldots$, for a selected Δt. We consider an observable of the states of the system (i.e., a smooth function f of x) and take $\{f(x(t_j))\}$ or $\{f(x(j))\}$ for $j = 0, 1, \ldots, N-1$ as the sample to be analyzed. If, after applying our Fourier analysis procedure, we are unable to obtain frequencies, we decide that the sample is not periodic nor quasi–periodic. If the orbit lives in a compact set, this lack of periodicity can be interpreted as the existence of some amount of chaos. On the contrary, if the sample displays a periodic or quasi–periodic behavior, then we can take another sample along the orbit (after a transient) and carry out the frequency analysis again. If the motion is regular the frequencies should be constant. Hence, we can set up a threshold for the admissible variation of the computed frequencies, and consider the motion as regular if the variation is less than the threshold.

In the present illustration we have considered a discrete system of the standard–like kind in dimension 2. More concretely, we study the family

$$T_{\varepsilon,\mu,\varphi}\begin{pmatrix} x \\ y \end{pmatrix} = \begin{pmatrix} \bar{x} \\ \bar{y} \end{pmatrix} = \begin{pmatrix} x + \varepsilon\bar{y} \\ y + \varepsilon f_{\mu,\varphi}(x) \end{pmatrix}, \tag{19}$$

where $f_{\mu,\varphi}$ is a 2π-periodic function with zero average. We shall take

$$f_{\mu,\varphi}(x) = g_{\mu,\varphi}(x) - \bar{g} \quad \text{with} \quad g_{\mu,\varphi}(x) = \frac{\sin(x+\varphi)}{1-\mu\cos(x)} \tag{20}$$

where $\bar{g}$ denotes the average of g, which is equal to $\sin(\varphi)\dfrac{\mu}{1-\mu^2+\sqrt{1-\mu^2}}$ (note that it is obtained from Eqs. (17, 18) by setting $k_j = \widetilde{\varphi}_j = 0$). We can take $\mu \in [0, 1)$ and $\varphi \in [0, 2\pi)$. There are several reasons to consider maps of the form of Eq. (19) with f as in Eq. (20):

- If $\mu = 0$, $\varphi = 0$ we recover the classical Taylor–Chirikov standard map.
- Some inconveniences of the classical standard map are that f is an *entire* function and that the effect of higher order harmonics is "too well averaged". This is avoided by taking $\mu > 0$, which implies that f has harmonics of all orders.
- The introduction of the phase φ destroys the symmetry of f.

The map given by Eq. (19) is also $2\pi/\varepsilon$-periodic in y. We can convert it to a map 2π-periodic in y by using the alternative version

$$\bar{x} = x + \bar{y} \bmod 2\pi, \quad \bar{y} = y + \varepsilon^2 f_{\mu,\varphi} \bmod 2\pi. \tag{21}$$

The expression given by Eq. (21) will be used in the sequel. Then, the map becomes a discrete dynamical system in the two-dimensional torus $\mathbb{T}^2$. We shall also fix $\mu = 0.5$, $\varphi = 1$ and, hence, we shall skip the dependence of f and T on μ and φ in Eqs. (19), (20). Fig. 6 displays a few phase portraits. From left to right (increasing ε) they show an increasing amount of stochasticity. We would like to have a compact representation of the full evolution for ε in a suitable range. We have used $\varepsilon \in [0, 1]$. It is clear that for $\varepsilon = 0$ the map given by Eq. (21) is integrable, all points being in invariant curves with rotation number going from 0 to 1 when y_0 ranges from 0 to 2π. Furthermore, it is clear from Eq. (19) that when $\varepsilon \to 0$ the phase portrait looks like a (distorted) pendulum.

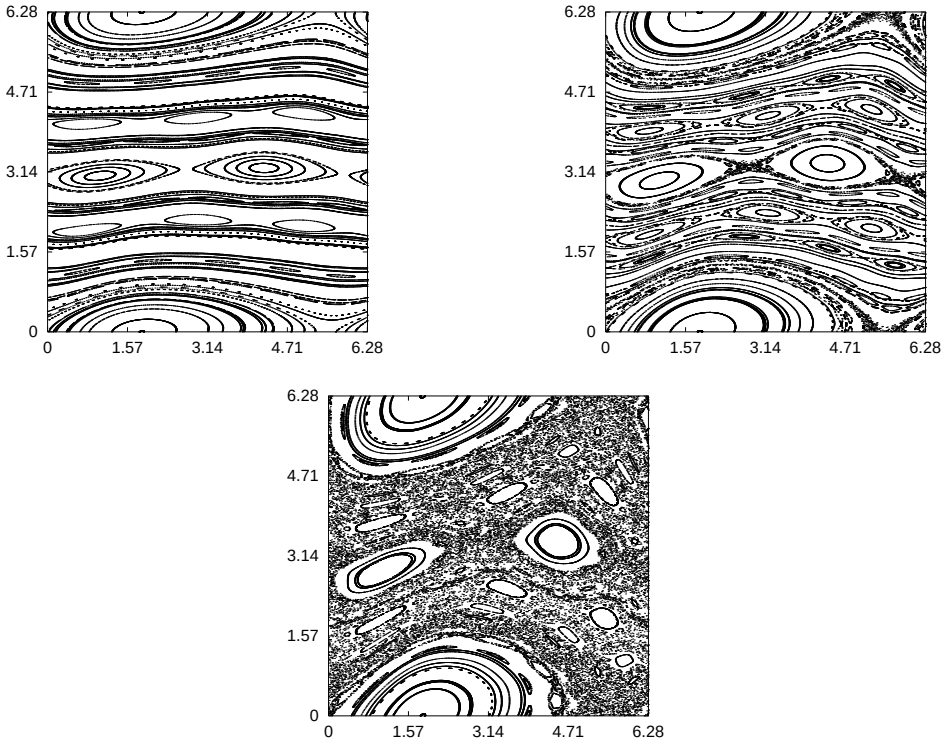

FIGURE 6. Phase portraits of the map given by Eq. (21). The horizontal (vertical) variable is x (y). From left to right and top to bottom we have used $\varepsilon = 0.4$, 0.6 and 0.8, respectively. In each plot we have taken $x, y \in \{2\pi j/10,\ j = 0, \ldots, 9\}$ and we have displayed the first 500 iterates.

5.1. **The numerical experiment.** For ε small it is enough to look at orbits with $x_0 = 0$ to describe essentially all the dynamics in $\mathbb{T}^2$. When ε increases, fixing $x_0 = 0$ implies that we shall miss several "islands", as can be seen in Fig. 6, but we still have a clear picture of the full dynamics if we confine x_0 to a fixed value. This is what we have done using values of ε of the form $j/1000$, $j = 1, \ldots, 1000$ and values of y_0 of the form $j2\pi/1000$, $j = 0, \ldots, 999$. For each one of these 10^6 cases we have analyzed the corresponding orbit using the procedure described in this paper.

We have used values of N of the form 2^k. Then $3 \times N$ additional iterates of T_ε have been done and we have analyzed again the last N. The selected observable is $\sin(x)$ (however see later for an additional observable). In principle we have studied the dominant frequency, that is, the one with the largest amplitude. An a priori value of the threshold for the difference of frequencies has been taken equal to 10^{-12}. We start with $k = 14$. If the orbit can be considered as regular the indices of the points are recorded as well as the frequency and the observed difference of the dominant frequencies in the two analysis. Otherwise k is increased up to a maximum of $k = 18$. If this value is reached then the dominant frequency and the difference of frequencies are written. In any case we have set up a maximal range for the values of y_j, which are considered in $\mathbb{R}$ without taking modulus 2π, in contrast with Fig. 6. If some iterate has y_j outside this range, then the orbit is considered as chaotic. A typical such range is $[-2\pi, 4\pi]$.

Two problems remain at this point. The first one is that the method is only able to determine frequencies in $(0, 1/2)$. Hence we are not able, for instance, to decide that an orbit lies in the main island around the elliptic fixed point or in the islands around the period 2 elliptic points (see Fig. 6). The second one is the ultimate selection of a threshold to decide about the regular or chaotic character of the orbits.

To solve the first problem a simple device is to consider the map of Eq. (21) in a slightly modified form which does not affect the dynamics. To this end we have considered the modified map $\hat{T}_\varepsilon$ given by

$$(\bar{x}, \bar{y}) = \hat{T}_\varepsilon(x, y), \quad \text{with} \quad \bar{x} = x + \bar{y} + 2\pi \bmod 10\pi, \quad \bar{y} = y + \varepsilon^2 f_{\mu,\varphi} \tag{22}$$

and as selected observable we have taken $\sin(x/5)$. In this way an initial frequency ω is transformed to $\hat{\omega} = (\omega + 1)/5$. As we obtain values $\hat{\omega} \in (0, 1/2)$ we can recover the full range $\omega \in [0 : 1]$. Furthermore, we use not only the dominant frequency in each run, but also the other frequencies obtained by the procedure (we have selected to detect, at least, the frequencies having the largest 10 amplitudes). From these frequencies we can compute basic frequencies such that all the remaining ones can be expressed as linear combinations of them. Hence, inside an island of a given period, it is possible to detect the rotation number of an invariant curve located in this island, or the periods of the islands which are satellites of a given island (either primary or secondary, etc, satellites).

The second problem was the ultimate selection of the threshold. To this end we have made tests against different indicators of the dynamics. The class of them known as *Lyapunov indicators* give a measure of the hyperbolicity in the vicinity of an orbit. The most classical is the *Lyapunov exponent*, which is defined as follows. Let $\{z_j,\, j = 0, 1, \ldots\}$ be an orbit of a discrete system, with $z_j = F^j(z_0)$. Let us take a random initial vector ξ on the tangent space at the point z_0 to the manifold $\mathcal{M}$ where F acts. Let $\xi_j = DF^j(z_0)\xi$ the vector obtained by the action of the differential on the tangent space. If $\mathcal{M}$ is Riemannian, for instance, we can measure the lengths on the tangent spaces. In our case this is trivial, the tangent spaces being $\mathbb{R}^2$. Assume $||\xi|| = 1$, where $||\ \ ||$ denotes any Riemannian metric. The Lyapunov exponent associated to the vector ξ along the orbit of z_0 is defined as

$$\lim_{j\to\infty} \frac{1}{j} \log(||\xi_j||). \tag{23}$$

The limit exists almost for all ξ and z_0 and it converges to the *maximal Lyapunov exponent* almost for all ξ and z_0. Note that the maximal Lyapunov exponent depends on z_0.

From Eq. (23) is it clear that a difficulty appears concerning the passage to the limit. Typically (i.e., except in systems which high instability) the behavior of the quotients in Eq. (23) is quite erratic. This is easy to understand if an orbit of a system like the one of Eq. (21) is mildly chaotic: the iterates of a point can remain until a large value of j close to a nearby chain of islands, to migrate then quickly to the vicinity of another chain of islands and remain there for a while. Furthermore this means that we are measuring an average of the hyperbolicity and not the *behavior of the dynamics near* z_0. This can be solved by taking final values of j not too large. They are a good measure of the *local properties* of the dynamics. It is also not necessary to compute the quotient nor the log in Eq. (23) if we are only interested in deciding whether the motion can be considered as chaotic or regular. Just to fix a maximal number of iterates J and a value L and decide that the orbit is chaotic if $||\xi_j|| > L$ for some $j \leq J$ or regular otherwise. Of course, depending on the selected values of J and L we shall consider as regular some orbits that are chaotic and vice versa. But this is unavoidable with finite computations and with finite accuracy. We refer to [12], [11] and references therein for an introduction to these ideas and examples. Alternative methods based on suitable filtering and weighting of data and on a deeper use of the dynamics can be found in [5, 9, 8, 38] and [28]. They are specially useful when not only the fact that the maximal Lyapunov exponent can be considered as positive is relevant, but when the interest is on the concrete numerical value.

Assuming we have selected J and L and decided about the character of a subset of the orbits analyzed by the Fourier procedure, we can find the most convenient threshold that minimizes the number of orbits which have been identified in a different way by both methods. This is the threshold that we shall use.

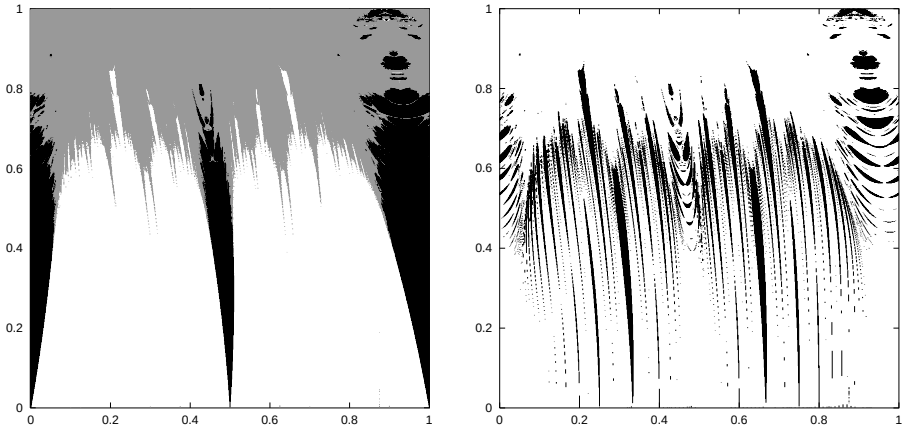

FIGURE 7. Results of the analysis of the map of Eq. (21). Left: the domain of chaotic behavior is shown in grey. All other pixels represent regular motion. In black the regular data having main frequency 0 or 1/2. Right: Domains of regular motion in an island. See the text for additional explanation.

5.2. **The results.** We proceed, as described above, using values $J = 10^6$ and $L = 10^{24}$ to set up the threshold. Smaller values can be used, but we wanted to be almost sure that the character decided by the Lyapunov indicator was correct. Using, say, $J = 10^4$ and $L = 10^6$, the fraction of wrong identifications is around 0.005, while with the selected values seems to be largely below 0.0001 . With these values the character of the different orbits has been compared to the one assigned by the Fourier procedure, which depends on the value of the threshold. Optimal results are produced for a threshold of 7×10^{-12}. Then the fraction of points with a lack of agreement is around 0.0018.

Figure 7 shows a graphical representation of the results. The scanning has been done using $x_0 = 0$. In the horizontal axis we represent $y_0/2\pi$ and in the vertical one the value of ε. On the left plot the grey domain means that a chaotic behavior has been found. Otherwise the orbits are regular. The black domains represent dynamics around the elliptic fixed point (domains to the left and right of the plot) or around the period 2 elliptic periodic orbit (central black part). The white pixels correspond to regular orbits, either on invariant curves or in islands of period greater than 2. On the right plot all the domains of regular motion in an island (periods have been limited to 100) are shown. In Fig. 8, it is illustrated the correspondence between a grey–tones–coded version of Figure 7 and the phase portrait of $\hat{T}_\varepsilon$ for $\varepsilon = 0.6$.

From Fig. 7 one can guess bifurcations and a fairly good idea of the full dynamics. This would change with the selected value of x_0, specially in what concerns the concrete location of the different islands, but this is not so relevant.

Finally, we would like to explain the main reasons of the observed disagreement between the Fourier and Lyapunov results, which affects roughly 1800 pixels among the 10^6. This number can be decreased if the size of the samples in the Fourier analysis is increased. To decide about the reasons, we have examined visually (with successive magnifications when required, with magnifying factors over 10^6 in some cases) around 500 different cases. In all of them visual inspection agrees with the character of the orbit assigned by the Lyapunov indicator.

A first source of disagreement relies in the *robustness* of the Fourier analysis mentioned at the end of Section 4. Indeed, a small chaotic zone near a chain of tiny islands of width below 10^{-6} can be not detected by the Fourier methods with the maximal sample size used. Another source of errors are invariant curves passing extremely close to a hyperbolic periodic orbit. Looking in a rough way at a significant number of iterates, it can seem that we are in a periodic orbit. Finally, there are motions on invariant curves (either rotational, i.e., projecting on the full x-axis, or librational, i.e., with several components around an elliptic periodic orbit) which look only as arcs of a curve if the number of iterates is small. The rotation number is too close to a rational.

For a further discussion on the suitability of the use of frequency analysis and/or Lyapunov exponents see Section 7.

6. **Study of the stability region of the planar RTBP around L_5.** This section is devoted to the application of the Fourier analysis procedure as a dynamical indicator in a problem that, although academic, is more complex than the preceding ones. The Fourier analysis procedure will be applied to the region of effective stability around the triangular points of the planar, circular Restricted Three–Body Problem in the Sun–Jupiter case, having as a goal the determination of the resonant

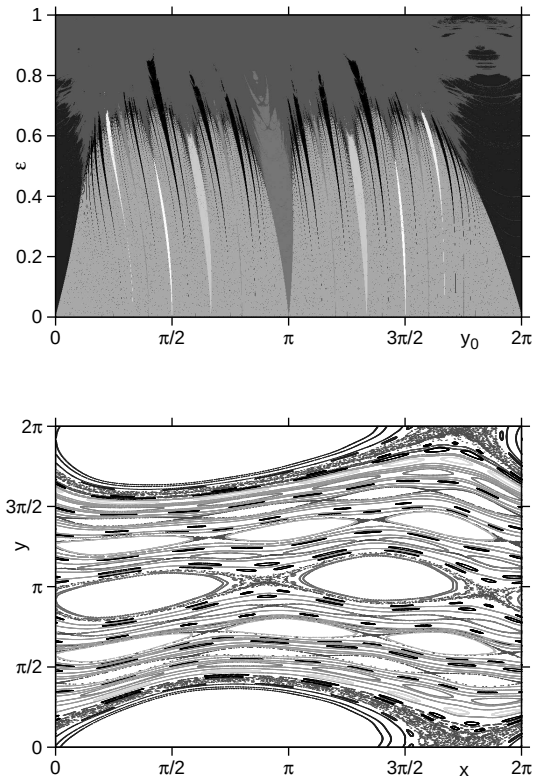

FIGURE 8. Top: grey–tones version, with less resolution, of Fig. (7) (both plots are merged). Bottom: phase portrait of the map $\hat{T}_\varepsilon$ for $\varepsilon = 0.6$. Each orbit shown has the color of the corresponding pixel in the top plot.

structure or this region, and to relate it to the frontier of the stability domain (see [30] for preliminary explorations of the regions of stable initial conditions around these points).

The planar, circular Restricted Three–Body Problem (RTBP) describes the motion of a particle considered massless (e.g. an spacecraft or an asteroid) under the gravitational influence of two massive ones (e.g. the Sun and a planet, or a planet and a moon). The two massive particles are called *primaries*. They are assumed to revolve uniformly in circles around their common center of mass. The RTBP depends on the *mass parameter* $\mu = m_2/(m_1 + m_2) \in (0, 1/2]$, where $m_1 > m_2$ are the masses of the primaries. It is usual to choose the distance between the primaries as length unit, and their period of revolution as 2π time units. It is also usual to consider a coordinate system that rotates with the primaries, so that they have have fixed positions on the x axis. In the equations we will use, the larger primary has coordinates $(\mu, 0)$, whereas the small one is located at $(\mu - 1, 0)$. The equations of

motion are

$$\begin{aligned} \ddot{x} - 2\dot{y} &= \partial_x \Omega(x,y), \\ \ddot{y} + 2\dot{x} &= \partial_y \Omega(x,y), \end{aligned}$$

where

$$\Omega(x,y) = \frac{1}{2}(x^2+y^2) + \frac{1-\mu}{r_1} + \frac{\mu}{r_2} + \frac{1}{2}\mu(1-\mu),$$
$$r_1 = \sqrt{(x-\mu)^2+y^2}, \quad r_2 = \sqrt{(x-\mu+1)^2+y^2}.$$

The RTBP is a autonomous 4D system of ODE that, introducing momenta as $p_x = \dot{x} - y$, $p_y = \dot{y} + x$, can be written in Hamiltonian form, with Hamiltonian

$$H(x,y,p_x,p_y) = \frac{1}{2}(p_x^2+p_y^2) - xp_y + yp_x - \frac{1-\mu}{r_1} - \frac{\mu}{r_2}.$$

More details can be found in classical books like [42].

The RTBP has five equilibrium points, called also Lagrangian or libration points, denoted as L_i, $i = 1,\ldots,5$. The three first ones are called *collinear* and lie in the line joining the primaries (the x axis). The $L_{4,5}$ points are called *triangular*, and form equilateral triangles with the primaries. The L_4 point precedes the secondary in its orbit around the primary, and therefore lies in the lower half–plane. The L_5 point is in the upper half–plane. See Fig. 9.

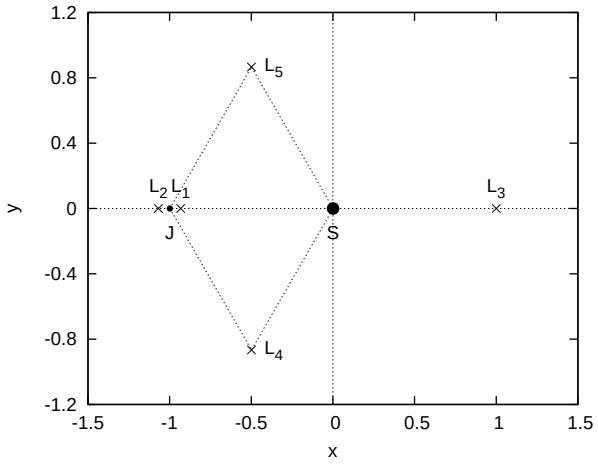

FIGURE 9. Primaries and equilibrium points for the circular, planar Sun–Jupiter RTBP in synodic coordinates.

From now on we will fix the mass parameter to the Sun–Jupiter one,

$$\mu = 1/1048.3486 = 9.5388118 \times 10^{-4}.$$

Our goal is to analyze the dynamics in the (effective) stability region around L_5. The linear behavior around L_5 is of the type center×center: if the first–order equations of the RTBP are denoted as $\dot{x} = f(x)$, we have

$$\operatorname{Spec} Df(L_5) = \{\pm i\omega_{\text{long}}, \pm i\omega_{\text{short}}\},$$

with

$$\omega_{\text{long}} = \left(\frac{1 - \sqrt{1 - 27\mu(1-\mu)}}{2} \right)^{1/2}, \quad \omega_{\text{short}} = \left(\frac{1 + \sqrt{1 - 27\mu(1-\mu)}}{2} \right)^{1/2}.$$

KAM–type results (see e.g. [24]) ensure the existence, sufficiently close to the equilibrium point, of (Cantorian) families of 2D tori. Since these 2D tori live in 3D energy levels, they separate space and thus enclose stability regions. Theoretically, these regions are only warranted to exist very close to the equilibrium point. They are known to be larger, at least from a practical point of view, since, for instance, Trojan asteroids can be found far from the L_5 equilibrium point of the Sun–Jupiter system. The existence of relatively large domains of stability in a "practical" sense, even in the 3D case, can be traced back to [15]. See [37] and [7] for improvements.

Numerical experiments allow to obtain more realistic estimations of the stability regions. One of such experiments, introduced in [17], is the following. Parametrize the neighborhood of L_5 by α, ρ as

$$\begin{pmatrix} x \\ y \end{pmatrix} = \begin{pmatrix} \mu \\ 0 \end{pmatrix} + (1+\rho) \begin{pmatrix} \cos(2\pi\alpha) \\ \sin(2\pi\alpha) \end{pmatrix}, \tag{24}$$

so that the L_5 point corresponds to $\alpha = 2/3$, $\rho = 0$. Choose a maximum integration time $T_{\max}$, and take an equally spaced grid of values of α, ρ in $[\alpha_{\min}, \alpha_{\max}] \times [\rho_{\min}, \rho_{\max}]$. Take initial conditions $x_0 = \mu + (1+\rho)\cos(2\pi\alpha)$, $y_0 = (1+\rho)\sin(2\pi\alpha)$, *with zero synodical velocity* $\dot{x}_0 = \dot{y}_0 = 0$ (note that they are not on the same value of the Jacobi constant), and try to numerically integrate them up to time $T_{\max}$ satisfying the following conditions:

(a) The trajectory shows no close approaches to the primaries.
(b) The (x, y) projection of the trajectory does not encircle the main primary.
(c) The (x, y) projection of the trajectory is never below a critical value of y, y_c.

If any of the three previous conditions is violated for $t < t_{\max}$, the corresponding point is considered to have escaped. The points that persist up to time $T_{\max}$ are considered to be in the practical stability region. The value $y_c = -0.5$ has been taken typically.

The points of Fig. 10 left have been obtained by the following refinement of the numerical experiment described above. In a first pass, all points that persist up to 2^{20} Jupiter revolutions ($T_{\max} = 2^{20} \times 2\pi$) are retained. The points of a grid in α, ρ with steps $\Delta\alpha = 5 \cdot 10^{-4}$ and $\Delta\rho = 5 \cdot 10^{-5}$ have been examined. The total domain scanned is large enough (around 0.6 Mpixel) to contain all the stable points around L_5. In a second pass, persistence is tested up to $\hat{T}_{\max} = 2^{24} \times 2\pi$. This is equivalent to almost 200 Myear in physical time. In order to reduce computing time, not all the points retained in the first pass are tested. Instead, consider all the pixels scanned in the first pass and assume that the pixels are marked as 0 or 1 according to whether they escape or not. Let (i, j) a pixel marked as 1. If some of the pixels in the range $[i-5, i+5] \times [j-5, j+5]$ is marked as 0, then this pixel is checked up to $\hat{T}_{\max}$, otherwise it is left with the mark 1. If the checked pixel escapes then it is marked as 0, otherwise as 2. The process is repeated for all the pixels marked as 1 and one keeps track of the number of pixels set to 0. After looking at all pixels, the process is repeated until a full passage through all the pixels marked as 1 (and that must be tested) do not leads to any additional escape. When this happens, it is reasonable to assume that the pixels that lie deeper into the 2^{20} stability region and are marked as 1 will also persist up to the larger time. They are "protected"

by a thick layer on points which do not escape for $t = \hat{T}_{\max}$. After the whole experiment, a total amount of 215115 points have subsisted. Fig. 10 displays this final practical stability region, in α, ρ (left) and synodic coordinates (right). Note that the "vertex" of the stability region is close to the equilibrium point L_3, which corresponds to $\alpha = \rho = 0$. This is due to the role played by the stable/unstable manifolds of the centre manifold around L_3 in defining the "boundaries" of the stable domain.

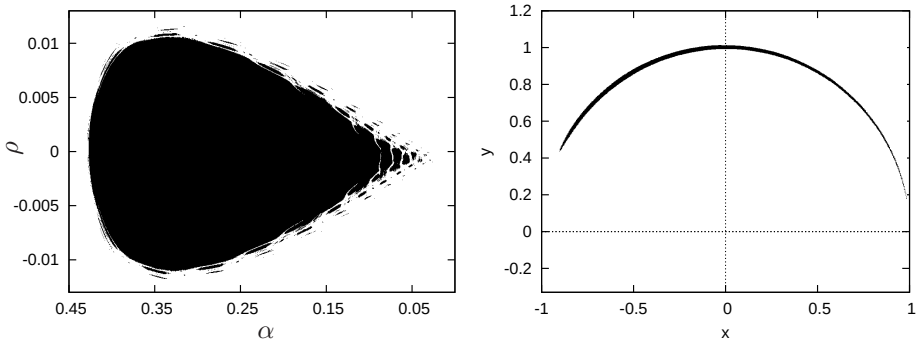

FIGURE 10. Effective stability region around L_5. Left: α, ρ coordinates of the subsisting points. Right: x, y coordinates of the same points.

It is worth to add a few comments on methods and CPU time. A high order Taylor method has been used with local truncation error of the order of the computer ϵ. Running on a Xeon processor at 3.20 GHz an average value of 180000 adimensional time units (more that 28000 Jupiter revolutions) takes just 1 second of CPU time. This means some 40^{s} (resp. 10^{m}) up to $T_{\max}$ (resp. up to $\hat{T}_{\max}$). Running on a cluster (HIDRA) where more than 200 programs can ran simultaneously, but some of the processors are slower, both the first pass and the iterative refinement take less than one day each. It is also relevant to mention that in the longest runs the total variation of the Jacobi constant has been checked to be below 10^{-13} and the standard deviation of the variations behaves as $t^{1/2}$, as corresponds to a random process. Taylor method is also extremely suitable to produce dense output at given multiples of a basic time interval.

Each of the subsisting points has been integrated again for $T = 65536$ time units ($65536/(2\pi)$ Jupiter revolutions), and the Fourier analysis procedure (Algorithm 3.1) has been applied to $N = 262144$ equally spaced samples of the x coordinate on the $[0, T]$ time interval, with Hanning order $n_h = 2$. The analysis have been stopped when either 30 frequencies have been detected or the minimum amplitude of the residual (starting trajectory minus its quasi–periodic approximation) has been under 10^{-6}. All the analysis have been completed in 49.69 hours of total CPU time, of which 25.69 hours have been spent in the numerical integration of the RTBP equations via Taylor's method, and the remaining 24 in Fourier analysis. The computation has been carried out in a cluster of 35 Xeon processors[2] at 3.00 GHz, so the elapsed time has been less than 1.5 hours. The frequencies of each

[2]Counting different cores as different processors.

analysis have been stored by decreasing amplitudes. The exit status of the Fourier procedure are summarized in Table 1.

status	#analysis	
OK	209556	97.42%
frequencies too close	4999	2.32%
iterative improvement (Subsect. 3.3) did not converge	395	0.18%
the two of the above	165	0.08%
TOTAL	215115	100%

TABLE 1. Summary of exit status of the Fourier exploration.

A comment must be made on frequency units: because of the use of the Fourier procedure, from now on all the frequencies will be given in cycles per unit of synodic time. In these units, the frequencies of the fixed point L_5 are

$$\nu_{\text{long}}^{L_5} = \omega_{\text{long}}^{L_5}/(2\pi) = 0.0128\,0626, \qquad \nu_{\text{short}}^{L_5} = \omega_{\text{short}}^{L_5}/(2\pi) = 0.1586\,3889.$$

Observe that $\nu_{\text{short}}/\nu_{\text{long}} = 12.3876$.

For each Fourier analysis, in Fig. 11 top left we have represented in red the frequency of maximum amplitude, and in blue the frequency of maximum amplitude in the range $[0.155, 0.165]$. Note that these frequencies are close to $\nu_{\text{long}}^{L_5}$ and $\nu_{\text{short}}^{L_5}$, respectively. Therefore, we will consider them to be the frequencies "propagated by continuity" (strictly, they are defined on a Cantor set) from the frequencies of the fixed point. They will be also denoted as $\nu_{\text{long}}, \nu_{\text{short}}$. Some additional facts in favor of this consideration are:

- If we scan all the analysis looking for the first frequency (in order of decreasing amplitudes) greater than 0.075, we obtain exactly the ν_{short} frequencies.
- The position in the frequency list (ordered by decreasing amplitudes) of the ν_{short} frequency is ≤ 5 in 203918 analysis (94.79%), ≤ 10 in 212395 analysis (98.74%), and ≤ 15 in 213819 analysis (99.40%).

If we represent the quotient $\nu_{\text{short}}/\nu_{\text{long}}$ along a line $\rho = \text{const}$ (Fig. 11 top right), we obtain the familiar devil staircase plot corresponding to the rotation number of a 2D area–preserving map around an elliptic fixed point. Note, though, that our practical stability region is **not** the phase portrait of such a map, since, for example, its points do not correspond to the same energy level, but span an interval of energies. In the devil staircase of Fig. 11 top right, we can distinguish flat pieces corresponding to the resonances 15,16,17,18.

We have post-processed the frequencies of each Fourier analysis with a routine implementing Algorithm 3.2, in order to extract a basic set. The parameters used have been $\text{tol} = 10^{-9}$, $\text{tol}_2 = 10^{-7}$, $k_{\max} = 100$, $m_{\max} = 2$. In all the Fourier analysis finished without an error exit code (first entry in Table 1), the routine implementing Algorithm 3.2 has taken the ν_{long} frequency as first basic frequency. The ν_{short} frequency has been taken as second basic frequency in 184829 analysis (85.92%). In 4132 additional analysis, in which the basis searching routine has not taken ν_{short} as second basic frequency, the ν_{short} frequency has non–zero component in the second basic frequency, so that it can enter the basis by a linear change. Then, the total number of analysis in which ν_{short} can be taken as second basic frequency amounts to 188961 (87.84%).

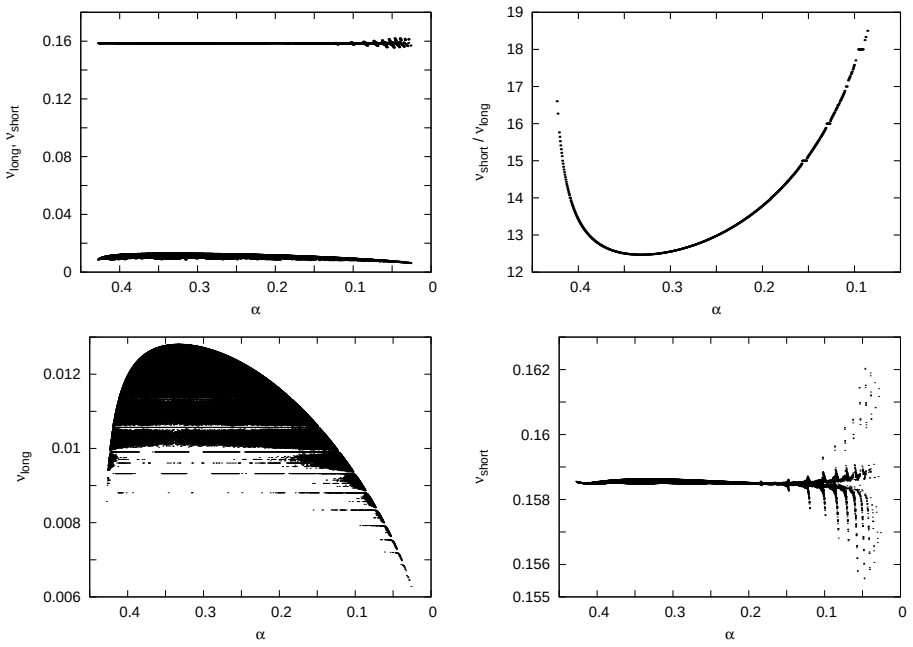

FIGURE 11. Top left: for all the analysis, maximum–amplitude frequency (ν_{long}) at the bottom of the plot, first frequency in the range $[0.155, 0.165]$ (ν_{short}) at the top of the plot. Top right: quotient of the two previous frequencies, for the analysis with $\rho = 4950$ only. Bottom: for all the analysis, detail of the ν_{long} (left) and ν_{short} (right) frequencies. On the left plot one can guess the location of the resonances. In all the plots the horizontal variable is the angle α as introduced in (24).

Fig. 12 summarizes all the results. In this figure:

(a) The analysis which have ended with an error code (entries 2,3,4 of Table 1) are represented in light grey (5559, 2.58%).
(b) The analysis not in (a) with an error $\geq 10^{-8}$ in the adjustment of frequencies as linear combination of basic ones are represented in grey (5882, 2.73%).
(c) The analysis not in (b) in which the ν_{short} frequency is not resonant with ν_{long} (that is, it can enter the basis) have been represented in dark grey (182630, 84.90%)
(d) The remaining analysis, that is, analysis not in (c) for which ν_{short} is a rational multiple of ν_{long}, are represented in black (21044, 9.78%).

Points in (a) and (b) may be related to diffusing (chaotic) orbits, either near the frontier of the stability region or within chaotic zones surrounding separatrices within the region (recall that, although we are describing Fig. 12 by analogy to a 2D area–preserving map, it does not correspond to such a map). The points in (c) correspond to non–resonant regular motion, whereas the points in (d) correspond to islands of regular, resonant motion. The first noticeable island chain corresponds to the 14:1 resonance, and, from this chain on, we find islands corresponding to higher–order resonances. From the resonance 16:1 on, some islands are disconnected from the

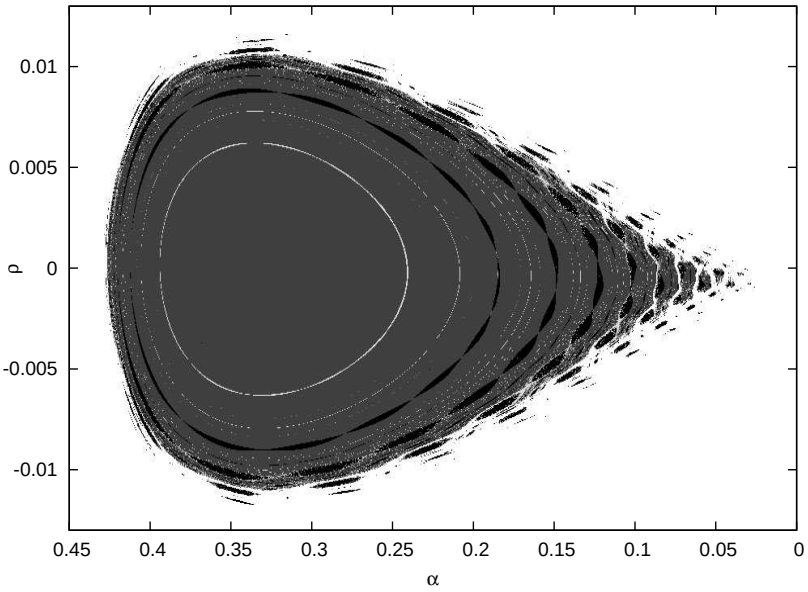

FIGURE 12. Resonance diagram of the (practical) stability region around L_5 for the planar, circular RTBP (see details in the text).

main stability region, and part of their associated separatrices are part of the frontier of the main stability region. The last detected resonance, which is 25:1, consists only of a few pixels hardly noticeable near the leftmost part of the plot. The islands corresponding to the 13:1 resonance are too dim for the resolution of this exploration. We can only distinguish in Fig. 12 a grey ring, with a few scattered green pixels, corresponding to orbits close to the corresponding separatrices.

7. **Performance and applicability.** This section is devoted to some comments on the applicability of frequency analysis and its comparison with other methods for similar purposes.

In the applications given in this paper, frequency analysis has been used as dynamical indicator. Compared to other dynamical indicators, frequency analysis allows not only to determine the character of the different orbits, but also to know the relevant frequencies and to locate and determine the resonances. If we are only interested in the character of the orbits and the location of the resonances, without a knowledge of the involved frequencies, then a Lyapunov indicator is faster. However, it is important to note that, in systems where numerical simulation is computationally more expensive than simple iteration (like the application in Section 6, where numerical integration of a system of ODE is needed), if the computing time required by frequency analysis is comparable to the time required for numerical simulation, the speed advantage of Lyapunov indicators is not so notorious. Mainly because the integration of the variational equations can largely increase the CPU time.

The Lyapunov indicator used in Section 5 is very fast but very simple, and requires several preliminary tests to adjust the J, L parameters for the distinction between regularity and chaoticity. This is specially critical in systems in which

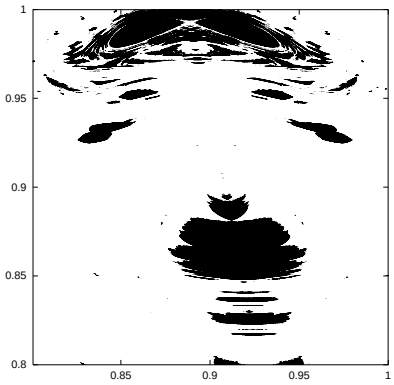

FIGURE 13. A magnification of the regular domain in Fig. 7 near the upper right corner.

the chaoticity is weak (or the time scales are long). To decide, for instance, if a computed Lyapunov exponent equal to 10^{-5} corresponds to a regular or a chaotic orbit, can be delicate. Other Lyapunov methods, like the one developed in [8], allow an accurate and fast determination of the character of the motion on their own. Fig. 13 shows a magnification of Fig. 7, done with the method of the previously mentioned references. This magnification corresponds to the regular domain for ε and $y_0/2\pi$ in $[0.8, 1]$, computed with step size 10^{-4} in both variables. It seems that a good strategy to learn about the properties of a dynamical system is to use a combination of Lyapunov indicators and frequency analysis. The additional use of other indicators, which take into account the dynamics, and continuation of relevant objects and their bifurcations, seems to be the optimal strategy (see [4], [6]).

A different application of the proposed procedures is the analytical construction of quasi–periodic models. Assume that a differential equation has a periodic or quasi–periodic (in time) external excitation but the form of the equations is rather cumbersome. An example of this situation is the motion of a spacecraft in a vicinity of the Earth-Moon system. The motion of both Earth and Moon and the effects of Sun (main perturbing body) but also the effects of other planets, can be assumed to be quasi–periodic for moderate time intervals (the chaotic behavior of the bodies in the solar system only becomes relevant after several million years, see [25]). Expanding the Hamiltonian of the problem around the Earth or the Moon, or around one of the instantaneous libration points, we obtain a Taylor series whose coefficients are quasi–periodic in time through the ephemeris of the bodies of the solar system. The expressions of the coefficients, as functions of the coordinates of the bodies, are known (see [18]). Using the refined Fourier analysis procedure presented in this paper, analytic models can be constructed. They reproduce in a faithful way the true equations of motion and are useful both for theoretical and massive numerical studies at a cheaper price than by using the current ephemeris. Work in this direction can be found in [20] and [32].

8. **Conclusions.** A numerical procedure for the accurate computation of frequencies and amplitudes of a quasi–periodic function from a regular sampling of it has been introduced. Some examples have been given in order to test its accuracy. Additional applications have been presented, showing its use as a dynamical indicator,

both in the distinction between regular and chaotic motion, and in the analysis of the structure of resonances. Its performance against other dynamical indicators has also been checked. A complete error analysis for this procedure is given in a separate paper [21].

Acknowledgments. The research has been supported by grants DGICYT BFM 2003-9504-C02-01, BFM2002-01344, MTM2005-02139, and MTM2006-05849/Consolider (Spain), together with CIRIT 2001 SGR-70, 2005 SGR-1028 (Catalonia). The authors are indebted to the referee for suggestions improving the readability of the paper.

REFERENCES

[1] V. I. Arnol′d, *Proof of a theorem of A.N. Kolmogorov on the preservation of conditionally periodic motions under a small perturbation of the Hamiltonian,* Uspehi Mat. Nauk, **18** (1963), 13–40.

[2] V. I. Arnol′d, V. V. Kozlov and A. I. Neĭshtadt, "Dynamical Systems. III," Encyclopaedia of Mathematical Sciences, vol. **3**, Springer-Verlag, Berlin, 1988.

[3] E. O. Brigham, "The Fast Fourier Transform and its Applications," Prentice–Hall, 1988.

[4] H. Broer, I. Hoveijn, M. van Noort, C. Simó and G. Vegter, *The parametrically forced pendulum: A case study in* $1 + \frac{1}{2}$ *degrees of freedom,* J. of Dynamics and Differential Equations, **16** (2004), 897–947.

[5] H. Broer and C. Simó, *Hill's equation with quasi–periodic forcing: resonance tongues, instability pockets and global phenomena,* Bul. Soc. Bras. Mat., **29** (1998), 253–293.

[6] H. Broer, C. Simó and R. Vitolo, *The Hopf-saddle-node bifurcation for fixed points of 3D-diffeomorphisms: Analysis of a resonance "bubble",* Physica D, **237** (2008), 1773–1799.

[7] A. Celletti and A. Giorgilli, *On the stability of the Lagrangian points in the spatial restricted problem of three bodies,* Cel. Mech., **50** (1991), 31–58.

[8] P. M. Cincotta, C. M. Giordano and C. Simó, *Phase space structure of multidimensional systems by means of the mean exponential growth factor of nearby orbits,* Physica D, **182** (2003), 151–178.

[9] P. M. Cincotta and C. Simó, *Simple tools to study global dynamics in non–axisymmetric galactic potentials – I,* Astronomy & Astrophysics Supp., **147** (2000), 205–228.

[10] M. Frigo and S. G. Johnson, *The design and implementation of FFTW3,* Proceedings of the IEEE, **93** (2005), 216–231.

[11] C. Froeschlé, M. Guzzo and E. Lega, *The fast Lyapunov indicator,* In "The Restless Universe" (eds. B. Steves and A. Maciejewski), IOP Publishing, (2001), 327–338.

[12] C. Froeschlé, E. Lega and R. Gonczi, *Fast Lyapunov indicators. Application to asteroidal motion,* Celest. Mech. and Dynam. Astron, **67** (1997), 41–62.

[13] D. Gabor, *Theory of communications,* J. Institute Electrical Engineering, **93** (1946), 429–457.

[14] C. Gasquet and P. Witomski, "Fourier Analysis and Applications," Filtering, numerical computation, wavelets, Translated from the French and with a preface by R. Ryan, volume **30** of Texts in Applied Mathematics, Springer-Verlag, New York, 1999.

[15] A. Giorgilli, A. Delshams, E. Fontich, L. Galgani and C. Simó, *Effective stability for a Hamiltonian system near an elliptic equilibrium point, with an application to the restricted three body problem,* J. Diff. Eq., **77** (1989), 167–198.

[16] G. Gómez, À. Jorba, C. Simó and J. Masdemont, "Dynamics and Mission Design Near Libration Point – Volume **3**: Advanced Methods for Collinear Points," World Scientific Monograph Series in Mathematics, 4, World Scientific Publishing Co., Inc., River Edge, NJ, 2001.

[17] G. Gómez, À. Jorba, C. Simó and J. Masdemont, "Dynamics and Mission Design Near Libration Point – Volume **4**: Advanced Methods for Triangular Points," World Scientific Monograph Series in Mathematics, 5, World Scientific Publishing Co., Inc., River Edge, NJ, 2001.

[18] G. Gómez, C. Simó, J. Llibre and R. Martínez, "Dynamics and Mission Design Near Libration Point Orbits – Volume **1**: Fundamentals: The Case of Collinear Libration Points," World Scientific, 2001.

[19] G. Gómez, J. Llibre, R. Martínez and C. Simó, "Dynamics and Mission Design Near Libration Point – Volume **2**: Fundamentals: The Case of Triangular Libration Points," World Scientific Monograph Series in Mathematics, 3, World Scientific Publishing Co., Inc., River Edge, NJ, 2001.

[20] G. Gómez, J. Masdemont and J. M. Mondelo, *Solar system models with a selected set of frequencies,* Astronomy & Astrophysics, **390** (2002), 733–749.

[21] G. Gómez, J. M. Mondelo and C. Simó, *A collocation method for numerical Fourier analysis of quasi–periodic functions. II: Analytical error estimates,* To appear in this journal, 2010.

[22] W. B. Jones and V. Petersen, *Continued fractions and Szegő polynomials in frequency analysis and related topics,* In "Proceedings of the International Conference on Rational Approximation," ICRA99 (Antwerp), Acta Appl. Math., **61** (2000), 149–174.

[23] À. Jorba and J. Villanueva, *On the normal behaviour of partially elliptic lower-dimensional tori of Hamiltonian systems,* Nonlinearity, **10** (1997), 783–822.

[24] À. Jorba and J. Villanueva, *On the persistence of lower–dimensional invariant tori under quasi–periodic perturbations,* Journal of Nonlinear Science, **7** (1997), 427–473.

[25] J. Laskar, *The chaotic motion of the solar system. A numerical estimate of the size of the chaotic zones,* Icarus, **88** (1990), 266–291.

[26] J. Laskar, *Introduction to frequency map analysis,* In "Hamiltonian Systems With Three or More Degrees of Freedom" (S'Agar, 1995), 134–150, NATO Adv. Sci. Inst. Ser. C Math. Phys. Sci., 533, Kluwer Acad. Publ., Dordrecht, 1999.

[27] J. Laskar, C. Froeschlé and A. Celletti, *The measure of chaos by the numerical analysis of the fundamental frequencies. Application to the standard mapping,* Physica D, **56** (1992), 253–269.

[28] F. Ledrappier, M. Shub, C. Simó and A. Wilkinson, *Random versus deterministic exponents in a rich family of diffeomorphisms,* J. of Stat. Phys., **113** (2003), 85–149.

[29] S. Mallat, "A Wavelet Tour of Signal Processing," Academic Press Inc., San Diego, CA, 1998.

[30] R. McKenzie and V. Szebehely, *Non-linear stability motion around the triangular libration points,* Celestial Mechanics, **23** (1981), 223–229.

[31] J. M. Mondelo, "Contribution to the Study of Fourier Methods for Quasi–Periodic Functions and the Vicinity of the Collinear Librations Points," PhD thesis, Universitat de Barcelona, 2001.

[32] E. Olmedo, "Càlcul de Solucions Quasiperiòdiques," Master's thesis, Universitat de Barcelona, Facultat de Matemàtiques, 2003.

[33] W. H. Press, S. A. Teukolsky, W. T. Vetterling and B. P. Flannery, "Numerical Recipes in C," Second edition. Cambridge University Press, Cambridge, 1992.

[34] C. Simó, *Boundaries of stability,* Talk given at the CSF conference, Universitat de Barcelona, Jun 3, 2006. Available at http://www.maia.ub.es/dsg/2006/.

[35] C. Simó, *Numerical experiences with Taylor methods,* Talk given at the "Geometric Integration Conference," Universitat Jaume I, Castelló, Sept 2, 2006. Available at http://www.maia.ub.es/dsg/2006/.

[36] C. Simó, *Properties of low dimensional dynamical systems in the large,* Lecture given at the workshop "Long Time Semiclassical Evolution," Wolfgang Pauli Institute, Vienna, Jan 8, 2007. Available at http://www.maia.ub.es/dsg/2007/.

[37] C. Simó, *Estabilitat de sistemes hamiltonians,* Mem. Real Acad. de Ciencias y Artes de Barcelona, (1989), 303–336.

[38] C. Simó, *Global dynamics and fast indicators,* In "Global Analysis of Dynamical Systems" (eds. H. Broer et al.), IOP Publishing, (2001), 263–289.

[39] C. Simó, G. Gómez, À. Jorba and J. Masdemont, *The bicircular model near the triangular libration points of the RTBP,* In "From Newton to Chaos" (Cortina d'Ampezzo, 1993), 343–370, NATO Adv. Sci. Inst. Ser. B Phys., 336, Plenum, New York, 1995.

[40] C. Simó, D. Puigjaner, J. Herrero and F. Giralt, *Dynamics of particle trajectories in a Rayleigh–Bénard problem,* Communications in Nonlinear Science and Numerical Simulation, **15** (2010), 24–39.

[41] C. Simó and A. Vieiro, *Towards a global study of area preserving maps. Examples, models and applications,* Slides of talks given at the workshops "Chaos and Ergodicity of Realistic Hamiltonian Systems," Centre de recherches mathématiques, Montréal, and "Workshop on

Mathematical Aspects of Celestial Mechanics," IHP and Observatoire de Paris, Paris, 2007. Available at http://www.maia.ub.es/dsg/2007/.

[42] V. Szebehely, "Theory of Orbits. The Restricted Problem of Three Bodies," Academic Press, 1967.

[43] L. Vela-Arévalo, "Time Frequency Analysis Based on Wavelets for Hamiltonian Systems," PhD thesis, California Institute of Technology, 2002.

[44] L. Vela-Arévalo and J. Marsden, *Time–frequency analysis of the restricted three–body problem: Transport and resonance transition,* Classical and Quantum Gravity, **21** (2004), 5351–5375.

Received September 2009; revised January 2010.

E-mail address: gerard@maia.ub.es
E-mail address: jmm@mat.uab.cat
E-mail address: carles@maia.ub.es